

CANCER

PTPN2 elicits cell autonomous and non-cell autonomous effects on antitumor immunity in triple-negative breast cancer

Pei Kee Goh^{1,2,3†}, Florian Wiede^{1,2,3†}, Mara N. Zeissig^{1,2,3†}, Kara L. Britt^{3,4}, Shuwei Liang^{1,2,3}, Tim Molloy⁵, Nathan Goode^{6‡}, Rachel Xu^{1,2,3}, Sherene Loi^{3,4}, Mathias Muller⁷, Patrick O. Humbert^{4,8,9,10}, Catriona McLean¹¹, Tony Tiganis^{1,2,3*}

The tumor-suppressor PTPN2 is diminished in a subset of triple-negative breast cancers (TNBCs). Paradoxically, PTPN2-deficiency in tumors or T cells in mice can facilitate T cell recruitment and/or activation to promote antitumor immunity. Here, we explored the therapeutic potential of targeting PTPN2 in tumor cells and T cells. PTPN2-deficiency in TNBC associated with T cell infiltrates and PD-L1 expression, whereas low PTPN2 associated with improved survival. PTPN2 deletion in murine mammary epithelial cells TNBC models, did not promote tumorigenicity but increased STAT-1-dependent T cell recruitment and PD-L1 expression to repress tumor growth and enhance the efficacy of anti-PD-1. Furthermore, the combined deletion of PTPN2 in tumors and T cells facilitated T cell recruitment and activation and further repressed tumor growth or ablated tumors already predominated by exhausted T cells. Thus, PTPN2-targeting in tumors and/or T cells facilitates T cell recruitment and/or alleviates inhibitory constraints on T cells to combat TNBC.

Copyright © 2022
The Authors, some
rights reserved;
exclusive licensee
American Association
for the Advancement
of Science. No claim to
original U.S. Government
Works. Distributed
under a Creative
Commons Attribution
NonCommercial
License 4.0 (CC BY-NC).

INTRODUCTION

Triple-negative breast cancer (TNBC), which accounts for 15 to 20% of all breast cancers, is an aggressive disease with poor outcomes when compared to hormone receptor or human epidermal growth factor receptor 2 (HER2)-positive breast carcinomas (1). As a consequence, considerable effort has been invested in defining new therapeutic avenues for TNBC. In the last few years, it has become clear that the immune system plays a critical role in influencing the course of TNBC disease progression and that approaches that engage the immune system, such as immune checkpoint-based therapies, can provide substantial benefit and enhance overall survival (1).

The presence of tumor-infiltrating lymphocytes (TILs), especially CD8⁺ T cells in TNBC, is associated with better prognosis and an increased chance of pathological complete response to chemotherapy (2–7). However, this can be influenced by the overall immune landscape and the abundance of immunosuppressive cells such as CD4⁺FOXP3⁺ regulatory T cells (T_{regs}) and myeloid-derived suppressor cells (MDSCs) within the tumor microenvironment (6). Along with CD8⁺ T cells, the expression of immune evasion molecules, such as PD-L1

(programmed death-ligand 1) on tumor cells and/or immune cells in the tumor microenvironment, can influence TNBC prognosis (8, 9). The engagement of inhibitory ligands, such as PD-L1, herpes virus entry mediator [HVEM; also known as TNF Receptor Superfamily Member 14 (TNFRSF14)], and major histocompatibility complex II (MHC-II) within tumors, with T cell inhibitory receptors such as programmed cell death protein-1 (PD-1), B and T lymphocyte attenuator (BTLA), and lymphocyte activation gene-3 (LAG-3) on T cells, promotes T cell tolerization or exhaustion and permits tumors to avoid immune destruction (8, 9). Nonetheless, the presence of TILs and the expression of immune evasion molecules such as PD-L1 afford unique opportunities for using immuno-modulatory approaches, such as those blocking the PD-L1/PD-1 immune checkpoint, which have been highly successful in the treatment of immunogenic tumors such as melanoma (8).

Exciting results from the phase 3 IMpassion130 trial comparing chemotherapy versus chemotherapy plus α-PD-L1 have underscored the potential for immune checkpoint blockade in combating TNBC (10). Patients with PD-L1⁺ TNBC in this trial derived an unprecedented overall survival benefit of 10 months (25 months versus 15.5 months; progression-free survival of 7.5 months versus 5 months). The poor prognosis for TNBC and unmet need culminated in the Food and Drug Administration granting accelerated approval for the use of α-PD-L1 in combination with paclitaxel for unresectable locally advanced or metastatic TNBC expressing PD-L1 (10). This represents the first immunotherapy treatment approved for breast cancer. Although only a subset of patients with TNBC derived significant benefit from α-PD-L1 therapy, the results of this trial substantiated the therapeutic potential of immunotherapy in TNBC.

Nonetheless, understanding the molecular basis for the heterogeneity in TIL abundance in TNBC and extending the utility of immunotherapy to patients that may otherwise have low TILs or engage alternate immune evasion strategies remain as major challenges (1). Previous studies have shown that activation of the Ras/MAPK

¹Monash Biomedicine Discovery Institute, Monash University, Clayton, Victoria 3800, Australia. ²Department of Biochemistry and Molecular Biology, Monash University, Clayton, Victoria 3800, Australia. ³Division of Cancer Research, Peter MacCallum Cancer Centre, Melbourne, Victoria 3000, Australia. ⁴Sir Peter MacCallum Department of Oncology, The University of Melbourne, Parkville, 3010, Australia. ⁵St. Vincent's Centre for Applied Medical Research, Darlinghurst, New South Wales 2010, Australia. ⁶Department of Biochemistry and Genetics, La Trobe Institute for Molecular Science, La Trobe University, Melbourne, Victoria 3086, Australia. ⁷Institute of Animal Breeding and Genetics, University of Veterinary Medicine Vienna, Vienna, Austria. ⁸Research Centre for Molecular Cancer Prevention, La Trobe University, Melbourne, Victoria 3086, Australia. ⁹Department of Biochemistry and Molecular Biology, University of Melbourne, Melbourne, Victoria 3010, Australia. ¹⁰Department of Clinical Pathology, University of Melbourne, Melbourne, Victoria 3010, Australia. ¹¹Anatomical Pathology, Alfred Hospital, Prahran, Victoria 3004, Australia.

*Corresponding author. Email: tony.tiganis@monash.edu

†These authors contributed equally to this work.

‡Present address: Pathology and Pathogenesis Group, CSIRO Australian Animal Health Laboratory, Geelong, Victoria 3220, Australia.

(mitogen-activated protein kinase) pathway after neoadjuvant chemotherapy decreases TILs and promotes immune evasion in TNBC by repressing signaling induced by interferon- γ (IFN γ) (11). IFN γ signals via Janus-activated kinase 1 (JAK-1) and JAK-2 and signal transducers and activators of transcription 1 (STAT-1) and STAT-3 (12). In breast cancer, increased STAT-1 Y701 phosphorylation (p-STAT-1) serves as an independent prognostic indicator of increased survival (13) and is associated with improved responses to chemotherapy (14), whereas increased *STAT1* mRNA is part of a molecular signature associated with improved metastatic outcome in estrogen receptor-negative (ER $^-$) tumors and TNBC (15). STAT-1 can not only directly repress the proliferation of breast cancer cells but can also act indirectly to promote T cell-dependent immune surveillance by driving the expression of T cell chemoattractants such as *CXCL9* and components of the antigen presentation machinery (16–19). In human breast cancer, *CXCL9* expression has been associated with increased TILs and improved survival (2). In addition, IFN-induced STAT-1 signaling drives the expression of *Cd274* (encodes PD-L1), *Tnfrsf14* (encodes HVEM), and *H2ab* (encodes MHC-II) (20, 21). Whereas the STAT-1-mediated expression of PD-L1 may render tumors amenable to PD-1 checkpoint blockade, the concomitant engagement of the BTLA4 and LAG-3 checkpoints (21) may diminish the effectiveness of α -PD-L1/ α -PD-1 therapy or ultimately render tumors resistant. Thus, approaches that generally enhance the recruitment and function of TILs and overcome the immunosuppressive tumor microenvironment may ultimately be more effective in combating TNBC than the targeting of individual checkpoints, such as PD-1.

One approach by which to bolster antitumor immunity in TNBC is to consider targeting protein tyrosine phosphatases (PTPs) such as PTPN2 (also known as T cell PTP or TCPTP) that can influence both T cell recruitment and T cell function (22–24). PTPN2 is a ubiquitous phosphotyrosine-specific phosphatase that predominantly exists as two variants in humans: a 48-kDa variant, which is targeted to the cytoplasmic face of the endoplasmic reticulum by a hydrophobic C terminus, and a shorter 45-kDa variant that is targeted to the nucleus and shuttles between the nuclear and cytoplasmic environments (25); a third less-common 41-kDa PTPN2 variant also exists and lacks both endoplasmic reticulum- and nuclear-targeting motifs (26). Both the 48- and 45-kDa PTPN2 variants can dephosphorylate and inactivate cytoplasmic substrates, such as Src family kinases (SFKs) and the JAK-1/3 protein tyrosine kinases (PTKs), whereas the 45-kDa nuclear variant can additionally dephosphorylate nuclear substrates, such as STAT-1, STAT-3, and STAT-5 in a cell context-dependent manner (25, 27–32). PTPN2 deficiencies in cell lines, xenografts, and genetically engineered mouse models of cancer promote PTK and STAT-3/5 signaling and tumorigenicity (32–34). In humans, PTPN2 is deleted in 6% of all T cell acute lymphoblastic leukemias (T-ALL) and is associated with increased NUP214-ABL1 and JAK/STAT oncogenic PTK signaling (35). Previously, using a validated monoclonal antibody (CF4) that specifically detected PTPN2 by immunohistochemistry, we reported that PTPN2 was also decreased in 28.5% (34 of 119) of breast cancers, including 44% (20 of 44) of ER $^-$ breast cancers and 67% (16 of 24) of TNBCs (34), whereas others have shown that PTPN2 is deleted in a subset of breast cancers (36, 37). The latter studies also used a polyclonal antibody to report that PTPN2 protein was low in 53.3% (354 of 664) of breast cancers and most commonly absent in ER $^-$ tumors (36, 37). We have shown that PTPN2 deficiency can promote PTK/STAT-3

signaling and the anchorage-independent growth of human breast cancer cells in vitro, as well the growth of human TNBC xenografts in immunocompromised nude mice (34). Moreover, we have reported previously that the absence of PTPN2 can also promote the development of hepatocellular carcinomas (32), whereas others have shown that PTPN2 deletion can facilitate skin carcinogenesis (33). Thus, PTPN2 can serve as a tumor suppressor in T-ALL and potentially solid tumors, including breast cancer. Nonetheless, recent studies have shown that PTPN2 deletion in syngeneic melanoma and colon tumors promotes IFN γ /JAK-1/STAT-1 signaling, T cell recruitment, and antigen presentation and enhances the response to PD-1 blockade (23). Moreover, other studies have shown that the deletion of PTPN2 in T cells promotes antitumor immunity by facilitating T cell activation and alleviating T cell exhaustion (22, 24, 38). In this study, we assessed the relative impact of PTPN2 deletion in mammary epithelial cells (MECs) and tumor cells on tumorigenesis versus antitumor immunity and explored the therapeutic potential of targeting PTPN2 in tumor cells and T cells to combat TNBC.

RESULTS

Low PTPN2 correlates with PD-L1 expression and T cell infiltrates in TNBC

The deletion of PTPN2 in syngeneic tumors and the promotion of IFN/JAK-1/STAT-1 signaling can increase antigen presentation and T cell recruitment and enhance the response to PD-1 therapy (23). We have reported previously that PTPN2 is not detected in a subset of ER $^-$ breast cancers and TNBCs (34). Therefore, we assessed whether low PTPN2 specifically in TNBC might be associated with increased TILs and PD-L1 expression. We monitored PTPN2 status by immunohistochemistry and TILs by histology and staining for CD3 ϵ , a component of T cell receptor (TCR) multisubunit signaling complex. To screen for PTPN2 in TNBC, we generated a monoclonal antibody (RE5a) to recombinant human 45-kDa PTPN2; RE5a recognized an epitope between residues 1 and 317, a region that incorporates the PTPN2 catalytic domain, which is identical in the PTPN2 variants (fig. S1, A and B). By immunoblotting, RE5a variably detected the 48- and 45-kDa variants of PTPN2 in human TNBC cell lines (fig. S1C); RE5a also detected the less-common 41-kDa PTPN2 variant in two of six TNBC cell lines (fig. S1C). Moreover, RE5a specifically detected PTPN2 by immunohistochemistry, as assessed by monitoring for PTPN2 immunoreactivity in sections from control HeLa tumor xenografts, as compared to those in which PTPN2 had been stably knocked down with a PTPN2-specific short hairpin RNA (shRNA) (fig. S1D). As noted previously (34), using RE5a, we could readily detect both nuclear and cytoplasmic localized PTPN2 in luminal and basal MECs in human mammary tissue (fig. S1E). We screened 28 TNBCs of which 9 were negative for PTPN2 (Fig. 1A, fig. S2, and table S1); for PTPN2-negative TNBCs, we confirmed the presence of PTPN2-positive lymphocytes as a control. Among TNBCs that were positive for PTPN2, both nuclear and cytoplasmic staining was evident (Fig. 1A and fig. S2). An analysis for intratumoral TILs revealed that seven of nine PTPN2-negative TNBCs had a TIL-predominated phenotype ($\geq 50\%$; $P < 0.0001$; Mann-Whitney U test), as assessed histologically (hematoxylin and eosin), whereas only 1 of 19 PTPN2-positive TNBCs had a TIL-predominated phenotype ($P = 0.0002$; Fisher's exact test) (Fig. 1B, fig. S2, and table S1). PTPN2-negative TNBCs that had high TILs also stained positive for CD3 ϵ , consistent with

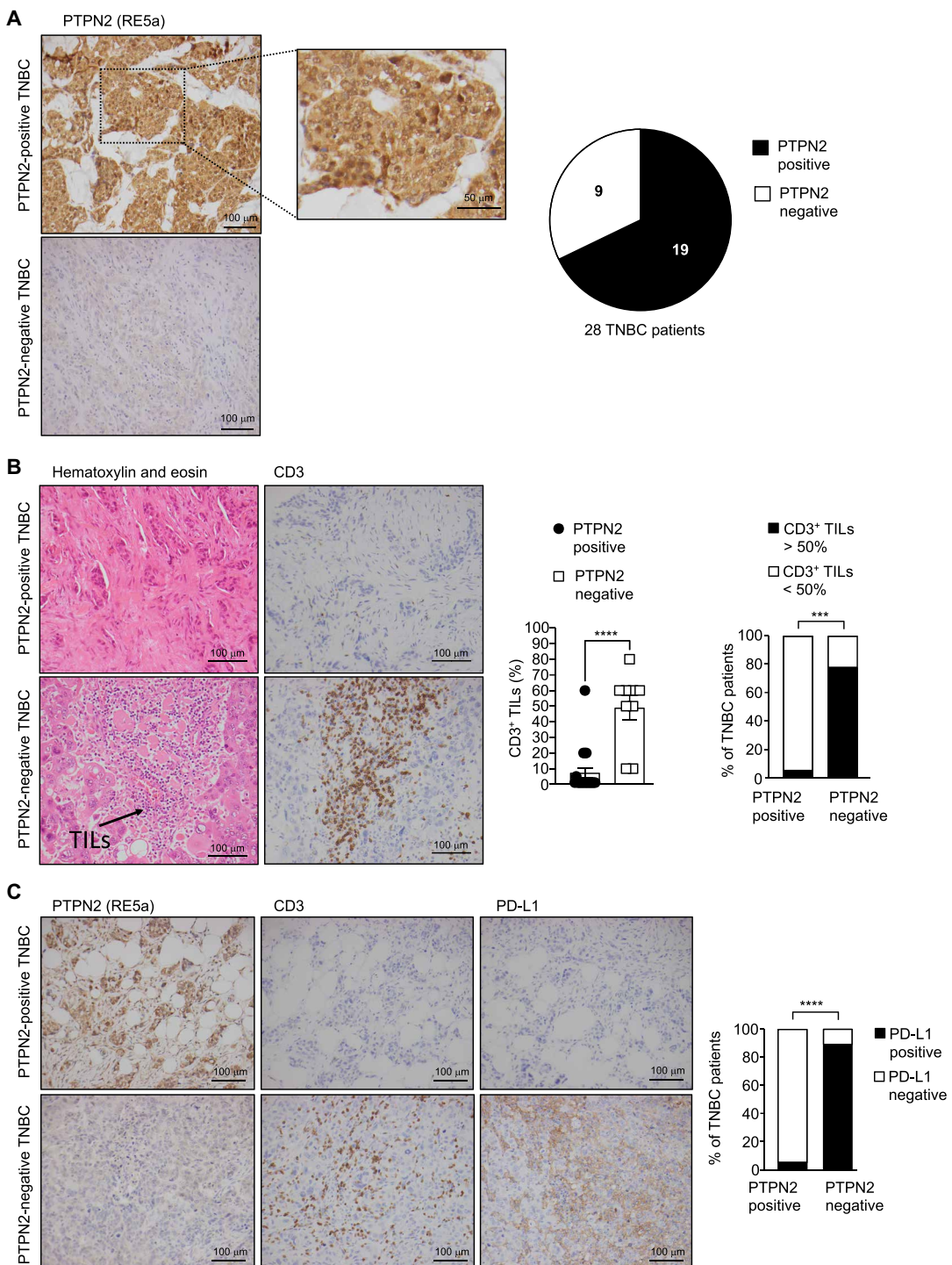


Fig. 1. PTPN2 deficiency in TNBC correlates with the presence of T cells and the expression of PD-L1. (A to C) Sections from formalin-fixed and paraffin-embedded TNBC tumors from 28 patients were deparaffinized, rehydrated, and processed for (B) histology (hematoxylin and eosin), and TILs were highlighted, or processed for (A to C) immunohistochemistry (counterstained with hematoxylin) and stained for PTPN2 (RE5a), CD3, or PD-L1. Representative images of PTPN2-positive and PTPN2-negative TNBCs are shown. Significance of CD3⁺ TILs in (B) was determined using two-tailed Mann-Whitney *U* test and, in (B and C), using Fisher's exact test; ****P* ≤ 0.001; *****P* ≤ 0.0001.

the infiltration of T cells (Fig. 1B and fig. S2). To determine whether the absence of PTPN2 in TNBC might promote STAT-1 signaling and the recruitment of T cells, we monitored for the STAT-1 transcriptional target PD-L1 (20) by immunohistochemistry. We found that the majority (8 of 9) of PTPN2-negative tumors stained

strongly for PD-L1, whereas only 1 of 19 of PTPN2-positive tumors stained for PD-L1 (*P* < 0.0001; Fisher's exact test) (Fig. 1C, fig. S2, and table S1). Therefore, PTPN2 deficiency in human TNBCs correlates with high PD-L1 expression and a preponderance of T cell infiltrates.

Low PTPN2 mRNA correlates with improved survival

Given the well-established positive correlation of T cell infiltrates with survival (2–7), we sought to explore the potential impact of low *PTPN2* expression on the survival of patients with breast cancer (Fig. 2). First, we interrogated a previously generated microarray gene expression dataset of 243 consecutively collected patients with stage I to III breast cancer (cohort 1) (39) as well as second microarray gene expression dataset from 462 patients with stage I to III breast cancer (The Cancer Genome Atlas; cohort 2) and correlated *PTPN2* expression to patient outcome and clinical variables. *PTPN2* expression in each case was normally distributed, and patients were split into quartiles of *PTPN2* expression for analysis. We found that those patients with *PTPN2* expression in the upper quartile had significantly

poorer breast cancer-specific survival than the patients with *PTPN2* expression in the lowest quartile [hazard ratio (HR) = 2.0 [95% confidence interval (CI) = 1.2 to 3.3], $P = 0.009$ by univariate Cox regression analysis for cohort 1 (Fig. 2A); HR = 2.1 (95% CI = 1.1 to 4.2), $P = 0.030$ for cohort 2 (Fig. 2B)]. Chi-square analyses showed that patients with high *PTPN2* mRNA expression had an increased likelihood of large (>20 mm) ER⁻, high-grade tumors of the basal-like (cohort 1; table S2A) or TNBC (cohort 2; table S2B) subtypes. Next, we specifically assessed the impact of low *PTPN2* mRNA expression on the survival of patients with TNBC. To this end, we interrogated a published microarray gene expression dataset of 238 patients with stage I to III TNBC (Fig. 2C) (40). Once more, patients with *PTPN2* expression in the upper quartile had significantly poorer survival

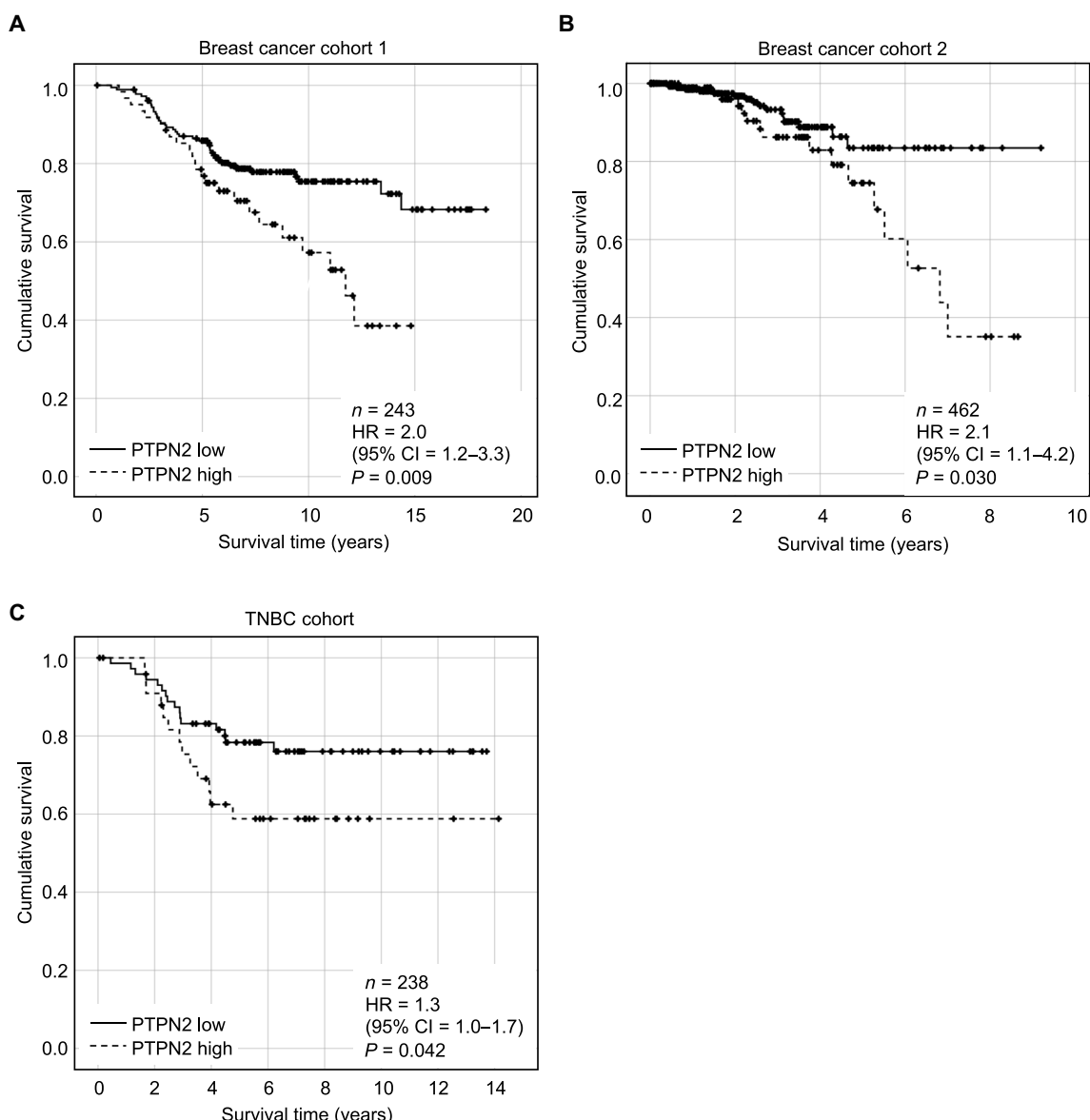


Fig. 2. Low PTPN2 mRNA expression is associated with improved breast cancer-specific survival. Microarray gene expression data from (A) tumors of 243 patients with stage I to III breast cancer (cohort 1), (B) 462 patients with stage I to III breast cancer (cohort 2), or (C) 238 patients with stage I to III TNBC was interrogated to correlate high and low *PTPN2* mRNA with survival. Times to disease-specific deaths were plotted as Kaplan-Meier survival curves. Cox proportional hazards regression was used for univariate analysis of the prognostic impact of *PTPN2* expression.

than patients in the lowest quartile [HR = 1.3 (95% CI = 1.0 to 1.7), $P = 0.042$ by univariate Cox regression analysis]. Therefore, low PTPN2 expression in breast cancer, including TNBC, is linked with improved survival.

PTPN2 deletion in MECs promotes hyperplasia and dysplasia but not tumors

Although PTPN2 deficiency may increase TILs and PD-L1 expression in TNBC and be associated with improved survival, the deletion of PTPN2 also has the potential to promote tumorigenicity by driving tyrosine phosphorylation-dependent signaling (32–35). Previous studies have shown that the deletion of PTPN2 in the liver or in the epidermis can promote STAT-3 signaling and tumorigenicity (32, 33). Accordingly, we assessed whether the deletion of PTPN2 in MECs might promote the genesis of cancer. Using an antibody (6F3) that specifically detects murine PTPN2 (fig. S3A), we found that nuclear PTPN2 was detected in luminal MECs in 4- to 10-week-old mice (fig. S3B) and throughout gestation (fig. S3C) and was also detected in cytokeratin 8 (CK8)-negative basal/myoepithelial cells (fig. S3D). Therefore, we deleted PTPN2 using the β -lactoglobulin (*BLG*)-Cre transgene that is activated in the alveolar luminal epithelial cells of the mammary gland with full recombination occurring after lactation (41). Although *BLG* is only expressed in luminal ER⁺ progenitors in virgin mice, expression occurs in basal and luminal cells after a pregnancy/lactation/involution cycle (42). Previous studies have used the *BLG*-Cre transgene to delete tumor suppressor genes in C57BL/6 mice and promote the formation of basal tumors (42, 43). Thus, we crossed *Ptpn2^{f/f}* (C57BL/6) with *BLG*-Cre (C57BL/6) mice and subjected the resulting *BLG*-Cre; *Ptpn2^{f/f}* mice to two rounds of pregnancy and processed inguinal mammary glands for histological analysis at least 3 weeks post-weaning; the deletion of PTPN2 in multiparous mice did not affect the survival of progeny at 21 days postpartum, consistent with mammary gland development and lactation not being overtly altered (table S3). PTPN2 was effectively deleted in MECs from multiparous mice, but only deleted in a subset of MECs in nulliparous mice, as assessed by immunohistochemistry (fig. S4); the efficient MEC deletion of PTPN2 in multiparous mice was also reaffirmed by flow cytometry (monitoring for PTPN2 in CD45[−]CD24⁺CD29^{lo} luminal and CD45[−]CD24⁺CD29^{hi} basal MECs; fig. S5). PTPN2 deletion in MECs was associated with increased STAT-3 signaling as assessed by STAT3 Y705 phosphorylation (p-STAT-3) and increased proliferation (Ki67 staining) as assessed by immunohistochemistry (fig. S6A). The mammary epithelium is organized into ducts and lobules and comprises CK8⁺ luminal and CK14⁺ basal cells arranged into bilayered structures; single layers of luminal cells line the lumen surrounded by basal/myoepithelial cells (44). The deletion of PTPN2 resulted not only in increased MEC proliferation but also in perturbations in the bilayer organization of mammary ducts, typified by the multilayering and intraductal growth of epithelial cells that was evident in a significant proportion of ductal-lobular structures (fig. S6B); aberrant mammary ducts were not evident in multiparous *Ptpn2^{f/f}* or *BLG*-Cre; *Ptpn2^{f/+}* controls (fig. S6C). We therefore subjected a cohort of 45 *Ptpn2^{f/f}* and 43 *BLG*-Cre; *Ptpn2^{f/f}* mice to five full-term pregnancies (with each cycle lasting approximately 2 months) with the intention of increasing the potential for tumor formation and processed mice for analyses at 1 year of age. No palpable tumors were detected in the aged *BLG*-Cre; *Ptpn2^{f/f}* mice. Histologically, no overt differences were evident in the overall density and distribution of mammary

ductal and alveolar structures, and there were no signs of hyperplastic nodules, characterized by focal aggregates of multilobular units. Notably, mammary ductal and alveolar structures did not show any signs of hyperplasia or the structural aberrations otherwise readily evident in younger *BLG*-Cre; *Ptpn2^{f/f}* mice after two rounds of pregnancy (fig. S7, A to C). Instead, mammary ductal and lobular structures were evident that were surrounded by CK8[−]CK14[−] infiltrates that included CD3ε⁺ T cells (fig. S7, B and C). Therefore, although PTPN2 deficiency can promote ductal-lobular hyperplasia and dysplasia in mice, this does not readily lead to the formation of mammary tumors. Instead, PTPN2 deficiency may concomitantly facilitate the recruitment of T cells to prevent tumor development.

PTPN2 deletion in MECs promotes STAT-1 signaling and T cell recruitment

We next explored the cell autonomous mechanisms by which the deletion of PTPN2 in MECs may facilitate T cell recruitment. To this end, we first bred *Ptpn2^{f/f}* (FVB/n) mice with MMTV-CreA (FVB/n) (45) mice to delete PTPN2 in both luminal and basal MECs in nulliparous mice (45), so that basal MECs could be isolated to analyze the impact of PTPN2 deficiency on ductal-lobular MEC outgrowths; basal MECs compose of mammary stem cells that are unique in their capacity to renew a mammary epithelial tree (46). PTPN2 was effectively deleted in MECs in nulliparous MMTV-CreA; *Ptpn2^{f/f}* mice (fig. S8A), and this was accompanied by increased p-STAT-3 (fig. S8B), proliferation (fig. S8C), and overt ductal dysplasia (fig. S8D), as also seen in multiparous *BLG*-Cre; *Ptpn2^{f/f}* mice (fig. S6B); aberrant mammary ducts were not evident in *Ptpn2^{f/f}* or MMTV-CreA; *Ptpn2^{f/+}* controls (fig. S9). Next, we adoptively transferred freshly isolated CD45[−]CD24⁺CD29^{hi} basal MECs (Fig. 3 and fig. S10, gating strategy) from 12-week-old *Ptpn2^{f/f}* (FVB/n) versus MMTV-CreA; *Ptpn2^{f/f}* (FVB/n) female mice into the cleared mammary fat pads of 3-week-old FVB/n female recipients (Fig. 3A) and monitored for the development of ductal-lobular MEC outgrowths after 12 weeks. No overt macroscopic outgrowth defects were evident (as assessed by whole-mount carmine alum staining; Fig. 3B), and engraftment was similar between the genotypes. As in multiparous *BLG*-Cre; *Ptpn2^{f/f}* (C57BL/6) female mice or nulliparous MMTV-CreA; *Ptpn2^{f/f}* (FVB/n) female mice, PTPN2 deficiency in transplanted FVB/n MECs resulted in increased p-STAT-3 and proliferation (Ki67 staining; Fig. 3C) and the expansion of CK8⁺ MECs so that the lumens of a large proportion of ducts and acini were filled with MECs (Fig. 3, D and E). Moreover, in some instances, CK8⁺ MECs in MMTV-CreA; *Ptpn2^{f/f}* outgrowths formed multiple layers detached from surrounding CK14⁺ basal cells (Fig. 3, D and E). Notably, the hyperplastic/dysplastic MMTV-CreA; *Ptpn2^{f/f}* MEC outgrowths were accompanied by a significant increase in host-derived PTPN2-positive and CK8/CK14-negative lymphocytic infiltrates (Fig. 4, A and B, and fig. S11A). A large proportion of the lymphocytic infiltrates that predominated the MMTV-CreA; *Ptpn2^{f/f}* MEC outgrowths were positive for the T cell marker CD3ε (Fig. 4C and fig. S11A), whereas B220⁺ B cells were evident in a small number of PTPN2-deficient MEC outgrowths (Fig. 4D and fig. S11A) as assessed by immunohistochemistry; using Opal multiplex immunohistochemistry, we found that the recruited T cells included both CD4⁺ and CD8⁺ T cells (fig. S11, B and C). Moreover, robust p-STAT-1 was evident in PTPN2-negative MMTV-CreA; *Ptpn2^{f/f}* MEC outgrowths (Fig. 4E and fig. S11A); the increased p-STAT-1 was not attributed to increased STAT-1 protein, as assessed by

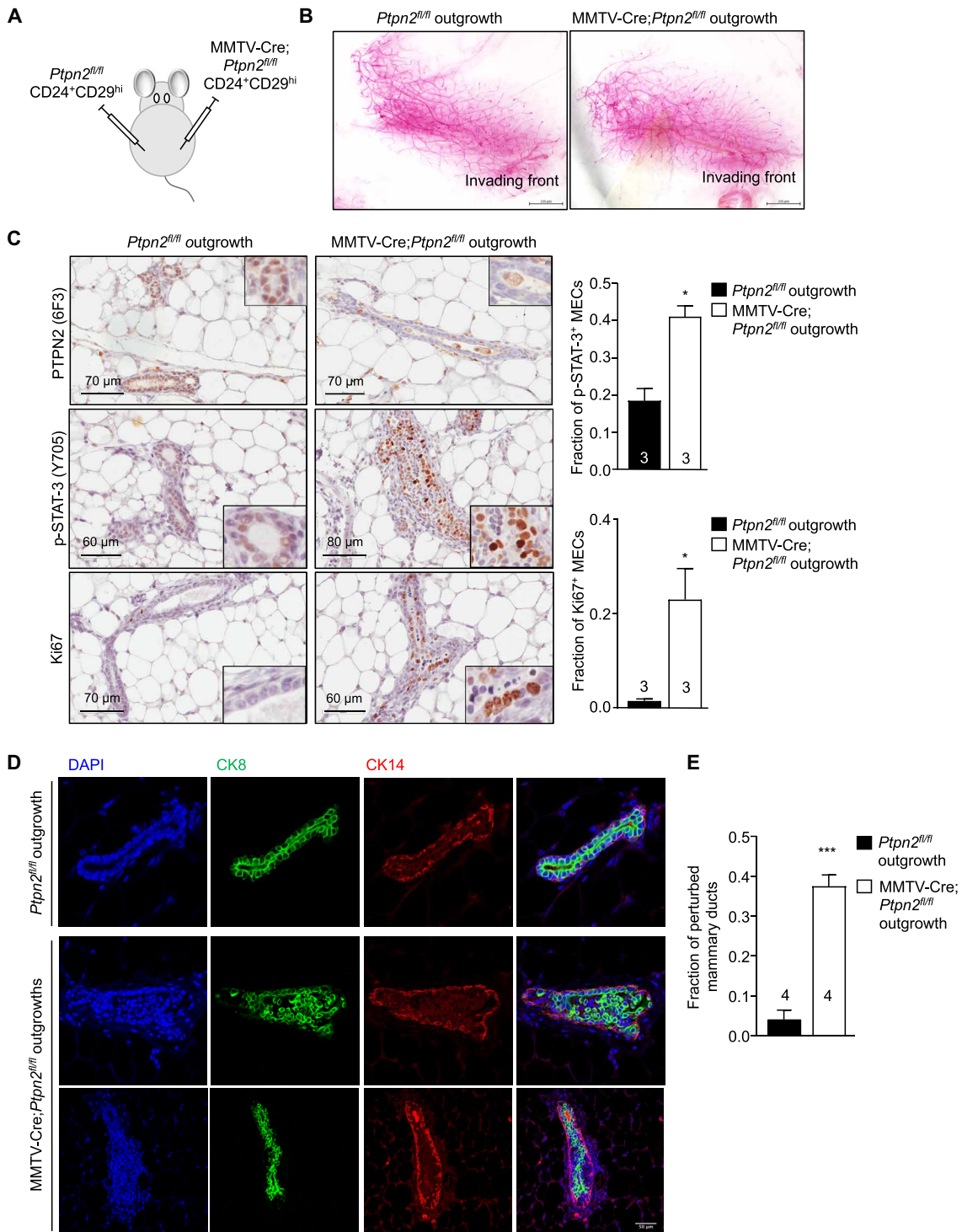


Fig. 3. Hyperplasia and dysplasia in PTPN2-deficient MEC outgrowths. (A) CD45⁻CD24⁺CD29^{hi} MECs were isolated from the mammary glands of 12-week-old *Ptpn2^{fl/fl}* and MMTV-Cre; *Ptpn2^{fl/fl}* females and transplanted contralaterally into the cleared mammary fat pads of 3-week-old FVB/n female mice. The transplanted fat pads were collected after 12 weeks and fixed in formalin, and (B) whole mounts stained with carmine alum to assess epithelial repopulation or processed for either (C) immunohistochemistry and stained for PTPN2, STAT-3 Y705 phosphorylation (p-STAT-3), and Ki67 (counterstained with hematoxylin) or (D) immunofluorescence microscopy and stained for CK8, CK14, and DNA [4',6-diamidino-2-phenylindole (DAPI)] to identify nuclei. In (C), p-STAT-3- or Ki67-positive MECs were quantified; three mice per genotype were scored, with three randomly selected fields of view scored per section. (E) Quantification of perturbed ductal structures in *Ptpn2^{fl/fl}* and MMTV-Cre; *Ptpn2^{fl/fl}* MEC outgrowths; four repopulated fat pads per mouse were scored per genotype with at least five randomly selected fields of view and 50 structures scored per gland. Results in (C) and (D) are means \pm SEM; significance was determined using two-tailed Student's t tests; *P \leq 0.05; ***P \leq 0.001.

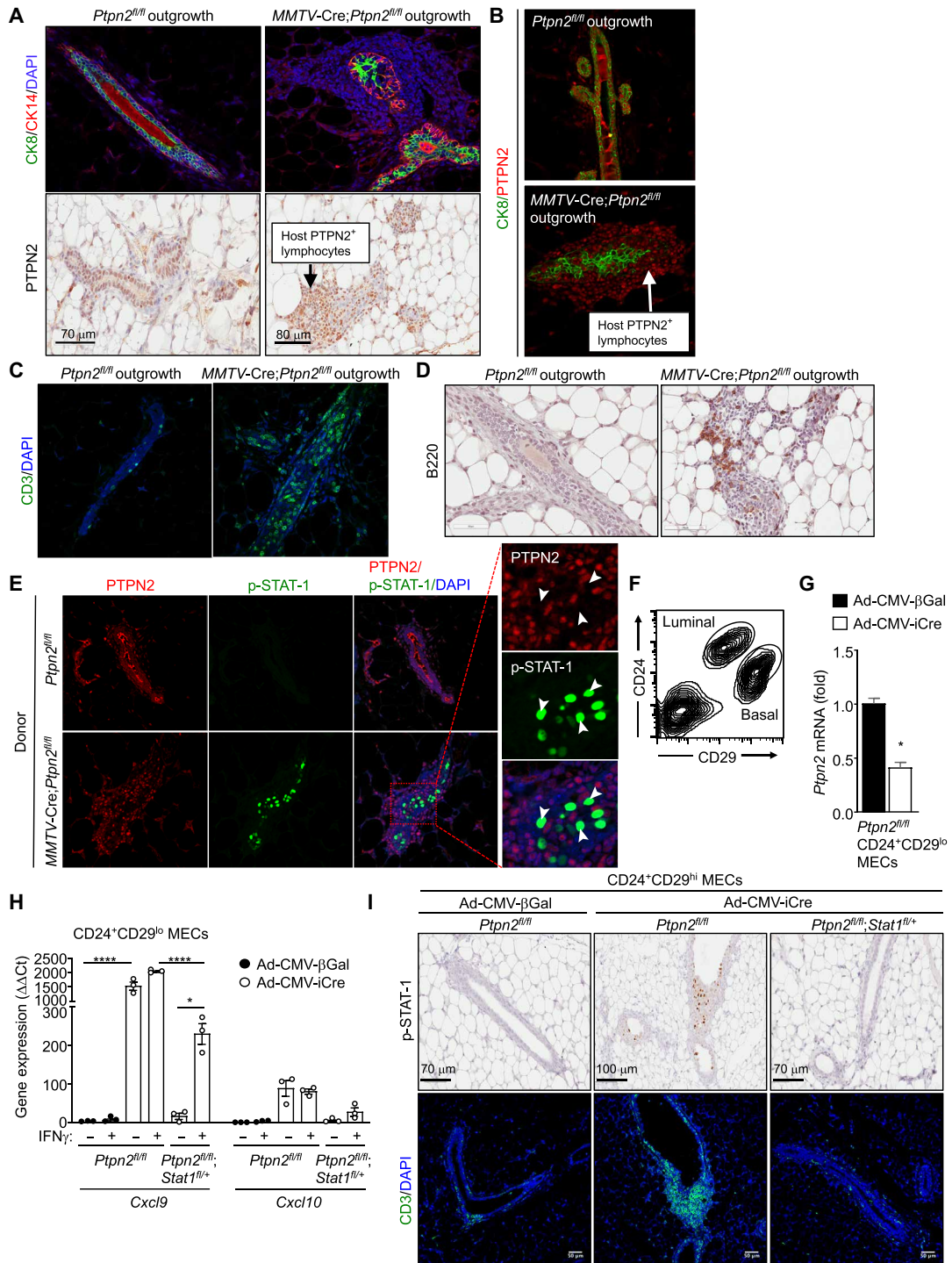


Fig. 4. PTPN2 deficiency promotes STAT-1 signaling and T cell recruitment in MEC outgrowths. (A to E) *Ptpn2^{+/+}* and *MMTV-Cre;Ptpn2^{+/+}* MEC mammary gland outgrowths were processed for immunohistochemistry (counterstained with hematoxylin) and immunofluorescence microscopy staining for PTPN2, CK8, CK14, CD3 (to mark T cells), B220 (to mark B cells), p-STAT-1, and DNA (DAPI). p-STAT-1 in PTPN2-negative *MMTV-Cre;Ptpn2^{+/+}* MECs are highlighted by arrowheads. (F) *Ptpn2^{+/+}* (C57BL/6) CD24⁺CD29^{hi} luminal MECs were purified by fluorescence-activated cell sorting, transduced with Ad-CMV-βGal or Ad-CMV-iCre and processed after 72 hours for quantitative real-time PCR (qPCR) to assess *Ptpn2* expression. (H) *Ptpn2^{+/+}* (C57BL/6) or *Ptpn2^{+/+};Stat1^{fl/fl}* (C57BL/6) CD24⁺CD29^{hi} luminal MECs were serum-starved and left untreated or stimulated with IFNγ (100 ng/ml, 72 hours) and processed for qPCR to assess *Cxcl9* and *Cxcl10* expression. Results are means \pm SEM from three independent experiments; significance in (G) was determined using two-tailed Student's *t* test and in (H) using two-way analysis of variance (ANOVA); **P* \leq 0.05; *****P* \leq 0.0001. (I) *Ptpn2^{+/+}* (C57BL/6) or *Ptpn2^{+/+};Stat1^{fl/fl}* (C57BL/6) CD24⁺CD29^{hi} basal MECs were transduced with Ad-CMV-βGal or Ad-CMV-iCre and were injected contralaterally into the cleared mammary fat pads of 3-week-old syngeneic C57BL/6 female recipients. After 12 weeks, MEC outgrowths were processed for immunohistochemistry monitoring for p-STAT-1 and CD3⁺ T cell infiltrates. Representative results from four to five repopulated fat pads per genotype per treatment are shown.

immunohistochemistry (fig. S12). Previous studies have established that the deletion of PTPN2 in tumor cells can enhance IFN γ /JAK-1/STAT-1 signaling and the expression of T cell chemoattractants such as C-X-C Motif Chemokine Ligand 9 (CXCL9), CXCL10, and C-C Motif Chemokine Ligand 5 (CCL5) to facilitate T cell recruitment (23). To determine the extent to which the heightened STAT-1 signaling in PTPN2-deficient MEC outgrowths may facilitate lymphocyte recruitment, we sought to correct the enhanced STAT-1 signaling by reducing the total amount of STAT-1 protein by 50%. To this end, we crossed *Ptpn2*^{fl/fl} (C57BL/6) mice onto the *Stat1*^{f/+} (C57BL/6) background and infected CD45 $^+$ CD24 $^+$ CD29 lo luminal MECs or CD45 $^-$ CD24 $^+$ CD29 hi basal MECs (Fig. 4F) from the resultant *Ptpn2*^{fl/fl}; *Stat1*^{f/+} versus *Ptpn2*^{fl/fl}; *Stat1*^{f/+} mice with adenoviruses expressing Cre recombinase (Ad-CMV-iCre) or β -galactosidase (Ad-CMV- β Gal) as a control. *Ptpn2* levels were reduced by approximately 60% (Fig. 4G), consistent with the adenoviral infection being suboptimal. Nonetheless, this was sufficient to markedly increase the expression of the STAT-1 target genes *Cxcl9* and *Cxcl10* (Fig. 4H), and this was largely corrected by *Stat1* heterozygosity. The corresponding infected basal MECs were transplanted into the contralateral cleared mammary fat pads of 3-week-old syngeneic C57BL/6 females and the impact on STAT-1 signaling and T cell recruitment assessment by immunohistochemistry after 12 weeks. As in MMTV-CreA; *Ptpn2*^{fl/fl} MEC outgrowths in FVB/n recipients, outgrowths arising from the transplantation of Ad-CMV-iCre-transduced *Ptpn2*^{fl/fl} MECs in C57BL/6 recipients had aberrant structures, including acini with filled lumens (fig. S13). In addition, Ad-CMV-iCre-transduced *Ptpn2*^{fl/fl} MEC outgrowths had higher p-STAT-1 and CD3 ϵ^+ T cell infiltrates than outgrowths from control *Ptpn2*^{fl/fl} MECs transduced with Ad-CMV- β Gal (Fig. 4I). *Stat1* heterozygosity largely corrected the increased p-STAT-1, otherwise associated with the deletion of PTPN2, as well as the recruitment of CD3 ϵ^+ T cells (Fig. 4I and fig. S14), but did not correct the aberrant acini (fig. S13) that likely arise from heightened PTK/STAT-3 signaling. Together, these results are consistent with PTPN2 deficiency in MECs promoting STAT-1 signaling and thereby T cell recruitment and antitumor immunity to eliminate aberrant ductal-lobular structures in the mammary gland that may otherwise develop into hyperplastic nodules and/or tumors with age.

PTPN2 deletion in mammary tumors variably promotes STAT-1-dependent T cell recruitment and antitumor immunity

Having established that the deletion of PTPN2 in MECs does not promote the development of mammary tumors, but instead may facilitate the recruitment of T cells and antitumor immunity, we thereon assessed the impact of PTPN2 deletion in mammary tumor cells. Specifically, we took advantage of syngeneic murine models of TNBC and assessed the influence of PTPN2 deletion on STAT-1 versus STAT-3 signaling and the impact on tumorigenicity versus antitumor immunity. To this end, we used CRISPR ribonucleoprotein (RNP)-based genome editing and a synthetic single guide RNA (sgRNA) to delete *Ptpn2* in AT3 adenocarcinoma cells, which form TNBC-like tumors when implanted into the mammary fat pads of mice; AT3 cells do not express ER, progesterone receptor (PR), or Erbb2 (murine HER2) and are derived from a mammary tumor arising in MMTV-PyMT transgenic FVB/n mice backcrossed onto the C57BL/6 (H-2^b) background (47). PTPN2 deletion enhanced both interleukin-6 (IL-6)-induced p-STAT-3 and IFN γ -induced p-STAT-1 (Fig. 5A) but did not overtly affect tumor cell

proliferation in vitro as assessed in colony-forming assays (fig. S15A). To assess the impact of PTPN2 deficiency on tumor growth in vivo, we implanted control and PTPN2-deficient AT3 mammary tumor cells into the inguinal mammary fat pads of syngeneic immunocompetent C57BL/6 mice (Fig. 5B). PTPN2 deletion increased nuclear p-STAT-1 and p-STAT-3 in AT3 mammary tumors in vivo as assessed by immunohistochemistry (Fig. 5C). Despite promoting STAT-3 signaling, PTPN2 deficiency suppressed the growth of AT3 syngeneic mammary tumors in vivo (Fig. 5B). The suppression of tumor growth was accompanied by a marked increase in the expression of STAT-1 target genes, including *Cxcl9* and *Cxcl10* (encoding CXCL9 and CXCL10), which facilitate lymphocyte recruitment (Fig. 5D and fig. S15B). On the other hand, the enhanced STAT-3 signaling was accompanied by the increased expression of the STAT-3 target genes *Il10* and *Ccl5*, which can facilitate tumor immune evasion (Fig. 5D). Nonetheless, in line with the increased *Cxcl9* and *Cxcl10* expression, PTPN2 deficiency in AT3 tumors was accompanied by increased lymphocyte infiltration, including CD3 ϵ^+ T cells, as assessed by immunohistochemistry (Fig. 5C). The increased lymphocyte recruitment included CD4 $^+$ and CD8 $^+$ effector/memory (CD44 hi CD62L lo) T cells and NK1.1 $^+$ natural killer (NK) cells that promote antitumor immunity (Fig. 5E and fig. S16, gating strategy), as well as immunosuppressive T_{regs}. PTPN2 deletion also increased the expression of other STAT-1 target genes, including *Tapb*, *Tap1*, and *H2k1* (encodes MHC-I) (Fig. 5D) that promote antigen presentation and *Cd274* (encodes PD-L1), *Hvem/Tnfrsf14* (encodes HVEM/TNFRSF14), and *H2ab1* (encodes MHC-II) (Fig. 5D and fig. S15B) that encode ligands for the PD-1, BTLA4, and LAG-3 checkpoints (12, 20, 21). Consistent with this, we found that PTPN2 deletion also significantly enhanced the response of AT3 tumors to PD-1 checkpoint blockade, where α -PD-1 was otherwise ineffective, and significantly increased survival (Fig. 6, A and B). Therefore, PTPN2 deletion in mammary tumors can promote STAT-1 signaling and T cell recruitment and repress tumor growth while also enhancing the response to immunotherapy.

To determine the extent to which the repression of AT3 tumor growth by PTPN2 deficiency might be ascribed to the recruitment of lymphocytes, we implanted control and PTPN2-deficient AT3 tumor cells into the mammary fat pads of *Rag1*^{-/-} (C57BL/6) mice that lack T cells and B cells and assessed tumor growth. Notably, tumor growth in immunocompromised *Rag1*^{-/-} mice was not significantly repressed by PTPN2 deficiency (Fig. 5F) despite increasing nuclear p-STAT-1 (fig. S15C). These results point toward the repression of tumor growth by PTPN2 deficiency in AT3 tumors in *Rag1*^{f/+} (C57BL/6) mice being attributable to the recruitment of lymphocytes. Therefore, these findings are consistent with PTPN2 deficiency in AT3 mammary tumors driving T cell recruitment and antitumor immunity.

Next, we assessed whether the heightened STAT-1 signaling in PTPN2-deficient AT3 tumors may be responsible for increased T cell recruitment and antitumor immunity. However, we first examined whether IFN expression may be increased in PTPN2-deficient AT3 mammary tumors to independently drive STAT-1 signaling and antitumor immunity. PTPN2 deficiency did not affect the expression of IFN α (*Ifna1*) or IFN β (*Ifnb1*) in AT3 tumors in either C57BL/6 or *Rag1*^{-/-} mice (Fig. 7A). By contrast, IFN γ expression (*Ifng*) was increased significantly in PTPN2-deficient AT3 tumors in C57BL/6 mice (Fig. 7A); the increased IFN γ expression was reliant on the recruitment of T cells, as it was not evident in *Rag1*^{-/-} mice.

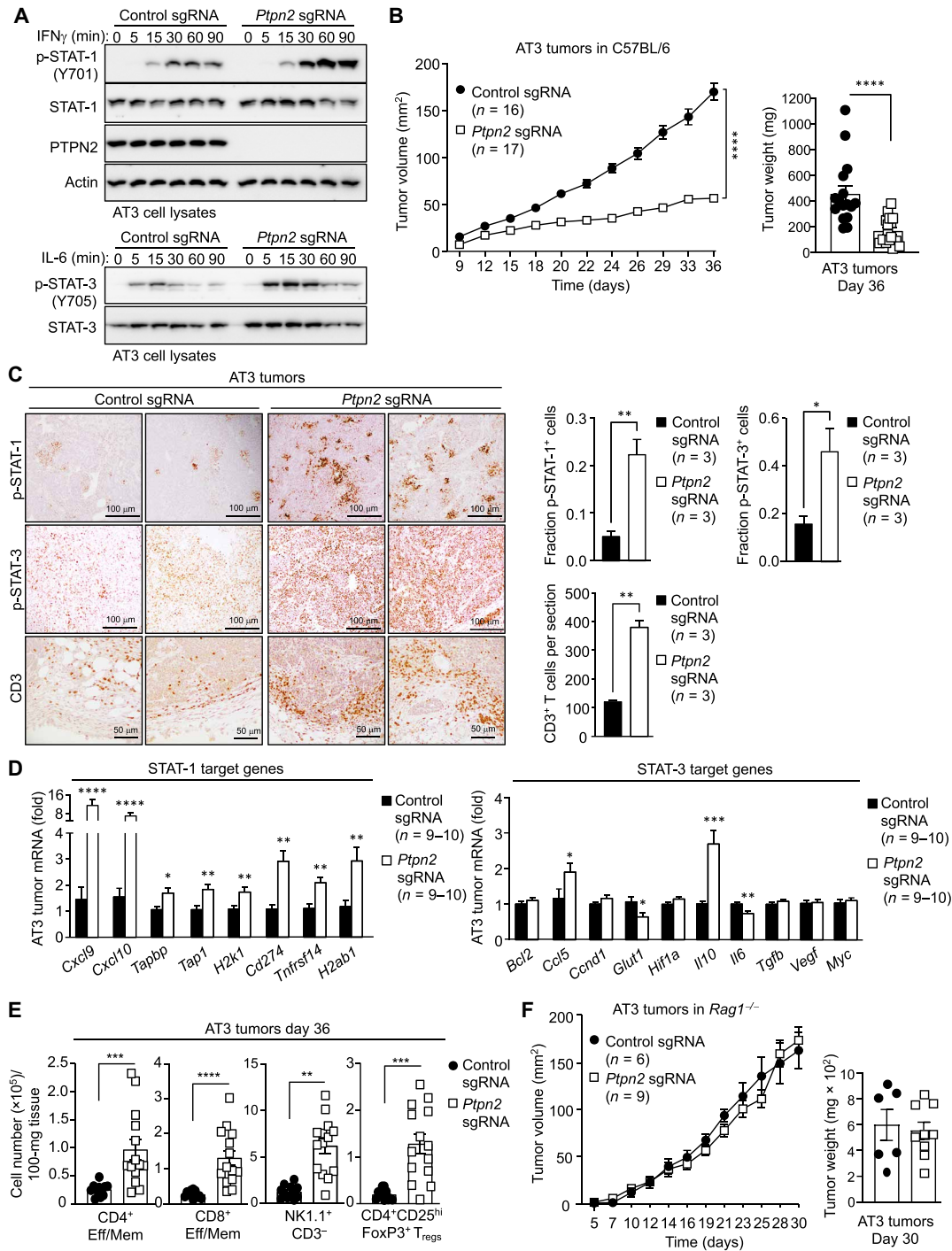


Fig. 5. PTPN2 deletion promotes STAT-1 signaling and the T cell-mediated repression of syngeneic AT3 mammary tumor growth in mice. (A) AT3 control cells (control sgRNA) or those in which PTPN2 had been deleted by CRISPR RNP (*Ptpn2* sgRNA) were stimulated with IFN γ or IL-6 for the indicated times. p-STAT-1, p-STAT-3, and PTPN2 protein levels were assessed by immunoblotting. (B to E) AT3 control or PTPN2-deficient cells were injected into the fourth inguinal mammary fat pads of female C57BL/6 mice, and (B) tumor growth was monitored. (C) Tumors were processed for immunohistochemistry staining for p-STAT-1, p-STAT-3, or CD3 (counterstained with hematoxylin). (D) mRNA expression of STAT-1 and STAT-3 target genes in AT3 tumors was assessed by qPCR. (E) The number of TILs including CD4 $^{+}$ and CD8 $^{+}$ T cells with a CD44 hi CD62L lo effector/memory (Eff/Mem) phenotype, NK1.1 $^{+}$ CD3 $^{-}$ NK cells, and CD4 $^{+}$ CD25 $^{+}$ FoxP3 $^{+}$ T_{reg}s were analyzed by flow cytometry. (F) AT3 control PTPN2-deficient cells were injected into the fourth inguinal mammary fat pads of female *Rag1*^{-/-} mice, and tumor growth was monitored. Representative results (means \pm SEM) from at least two independent experiments are shown. In (B) and (F), significance was determined using two-way ANOVA test and, in (D) and (E), using two-tailed Mann-Whitney *U* test. For tumor weights in (B), significance was determined using two-tailed Mann-Whitney *U* test. In (B) and (F), tumors were analyzed at end point. In (C), results are representative of five mice per group, and images were taken at $\times 10$ (p-STAT-1 and p-STAT-3) or $\times 20$ (CD3) magnification; sections from three mice per group were scored with three fields of view scored per section, and significance was determined using two-tailed Student's *t* test, * $P \leq 0.05$; ** $P \leq 0.01$; *** $P \leq 0.001$; **** $P \leq 0.0001$.

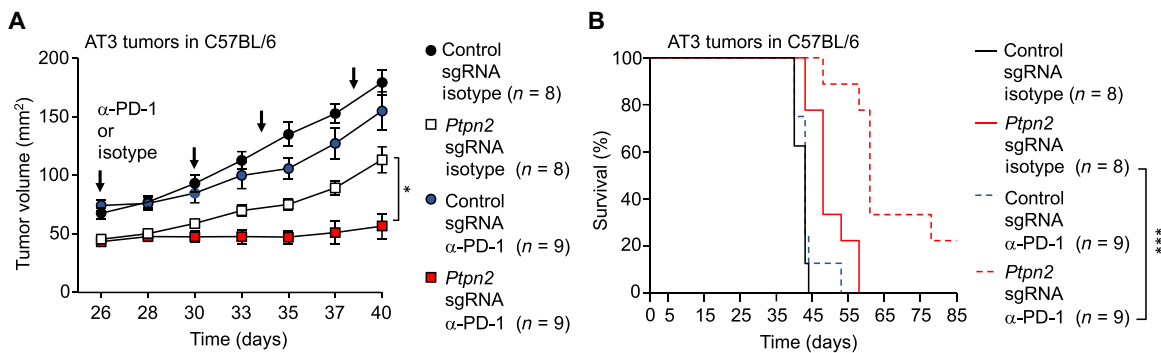


Fig. 6. PTPN2 deficiency in AT3 mammary tumors enhances the efficacy of α-PD-1 therapy and extends survival. (A and B) AT3 control cells (control sgRNA) or those in which PTPN2 had been deleted by CRISPR RNP (*Ptpn2* sgRNA) were injected into the fourth inguinal mammary fat pads of female C57BL/6 mice. Mice were treated with α-PD-1 or isotype control on days 26, 30, 34, and 38, and (A) tumor growth and (B) survival were monitored. Representative results (means ± SEM) from two independent experiments are shown. In (A), significance was determined using two-way ANOVA test and, in (B), using a log-rank (Mantel-Cox) test; *P ≤ 0.05; **P ≤ 0.001.

This was not unexpected, as T cells, along with NK cells, are major sources of IFN γ in tumors and PTPN2 deficiency in AT3 tumors increased T cell recruitment. These results indicate that the increased STAT-1 signaling and T cell recruitment in PTPN2-deficient AT3 tumors cannot be attributed to increased tumor IFN production, but rather may be an outcome of enhanced responses to cytokines, as noted in vitro (Fig. 5A). Next, we sought to attenuate STAT-1 signaling in PTPN2-deficient tumors. Specifically, we determined whether blocking the type I IFN (IFN α/β) receptor IFNAR1 in PTPN2-deficient AT3 tumors might repress STAT-1 signaling, because PTPN2 deficiency resulted in increased p-STAT-1 in AT3 tumors even in *Rag1*^{-/-} mice (fig. S15C), where IFN γ expression was negligible (Fig. 7A). Mice with palpable PTPN2-deficient AT3 mammary tumors were injected with α-IFNAR1 every 3 days, and effects on tumor growth were assessed (Fig. 7B). The blockade of IFNAR1 signaling significantly attenuated the repression of tumor growth otherwise achieved with the deletion of PTPN2 in AT3 tumor cells (Fig. 7B). This was accompanied by decreased nuclear p-STAT-1, as assessed by immunohistochemistry (fig. S17A); repressed STAT-1 target gene expression (Fig. 7C); and repressed T cell and NK cell recruitment, as assessed by flow cytometry or CD3 immunohistochemistry (Fig. 7, D and E). In keeping with the repressed T cell recruitment, IFN γ (*Ifng*) expression was also reduced by the blockade of IFNAR1 signaling (Fig. 7C). Therefore, PTPN2 deficiency and the promotion of IFN α/β signaling in tumors can facilitate the recruitment of T cells.

To directly assess the contributions of STAT-1, we took advantage of CRISPR RNP gene editing and specific sgRNAs to delete *Stat1* in PTPN2-deficient AT3 tumor cells (fig. S17B). The deletion of *Stat1* largely ablated the IFN γ -induced expression of STAT-1 target genes including *Cxcl9*, *Cxcl10*, and *Cd274* in vitro (fig. S17C). Moreover, the deletion of *Stat1* attenuated the repression of tumor growth otherwise achieved with PTPN2 deficiency (Fig. 8A). This was accompanied by the repressed expression of STAT-1 target genes, including T cell/NK cell chemoattractant (*Cxcl9* and *Cxcl10*), immune checkpoint ligand (*Cd274*, *Tnfrsf14*, and *H2ab1*), and antigen presentation (*Tapb*, *Tap1*, and *H2k1*) genes (Fig. 8B). This was also accompanied by the repression of T cell and NK cell recruitment as assessed by flow cytometry (Fig. 8C) or CD3ε immunohistochemistry (Fig. 8D). These results are consistent with PTPN2 deficiency increasing T cell recruitment and antitumor immunity and repressing AT3 mammary tumor growth by promoting the IFN-STAT-1

signaling axis. These findings are consistent with previous studies demonstrating that the deletion of PTPN2 in syngeneic MC38 colon carcinomas or B16F10 melanomas can also increase STAT-1 signaling and T cell recruitment, albeit by promoting the response to IFN γ to promote antitumor immunity (23), a finding that we have also recapitulated.

Although our findings point toward PTPN2 deficiency in TNBC driving T cell recruitment, a small subset of PTPN2-positive TNBCs nonetheless have high TILs (Fig. 1). Accordingly, we also sought to assess the impact of deleting PTPN2 in a syngeneic mammary tumor model with high TILs. To this end, we deleted PTPN2 in murine E0771 adenocarcinoma cells, which originate from a spontaneous medullary mammary tumor in a C57BL/6 mouse (48). E0771 cells grow aggressively when implanted into the mammary fat pads of mice and are predominated by TILs, a robust immunosuppressive tumor microenvironment with abundant MDSCs and T_{reg}s and high levels of PD-L1 (24, 49). Orthotopic E0771 mammary tumors resemble human TNBC as they are ER-, PR-, and ErbB2-negative, mutant for *TRP53* and have basal-like characteristics (48). As with AT3 cells, PTPN2 deletion in E0771 cells using CRISPR RNP gene editing resulted in enhanced IL-6-induced STAT3 signaling and IFN γ -induced STAT-1 signaling in vitro (fig. S18A). However, p-STAT-1 was already increased in E0771 mammary tumors when compared to AT3 tumors in vivo, and this was only moderately, if at all, increased by PTPN2 deficiency (Fig. 9A). This coincided with significantly increased IFN β levels in E0771 versus AT3 tumors, as well as heightened IFN γ expression in E0771 tumors that was unaffected by PTPN2 deficiency and approximated that seen in PTPN2-deficient AT3 tumors (Fig. 9B). Consistent with the heightened IFN β/γ expression and p-STAT-1, the STAT-1 target genes *Cxcl10* and *Cd274* (PD-L1) were increased in control E0771 versus AT3 mammary tumors in vivo (Fig. 9C). The expression of *Cxcl10* and *Cd274* in control E0771 tumors approximated that in PTPN2-deficient AT3 tumors (Fig. 9C). PTPN2 deficiency in E0771 mammary tumors moderately increased *Cxcl9* expression (fig. S19A), but other STAT-1 target genes, including *Cd274*, were decreased rather than increased (fig. S19A). Unlike in AT3 tumors (Fig. 5C), PTPN2 deficiency in E0771 tumors did not result in significant differences in p-STAT-3 as assessed by immunohistochemistry (fig. S18B) and did not overtly influence the proliferation of cells in vivo as assessed by Ki67 staining (fig. S18B). Moreover, PTPN2 deletion had no effect on the growth rates of E0771 mammary tumors in C57BL/6 mice (fig. S19B) and it

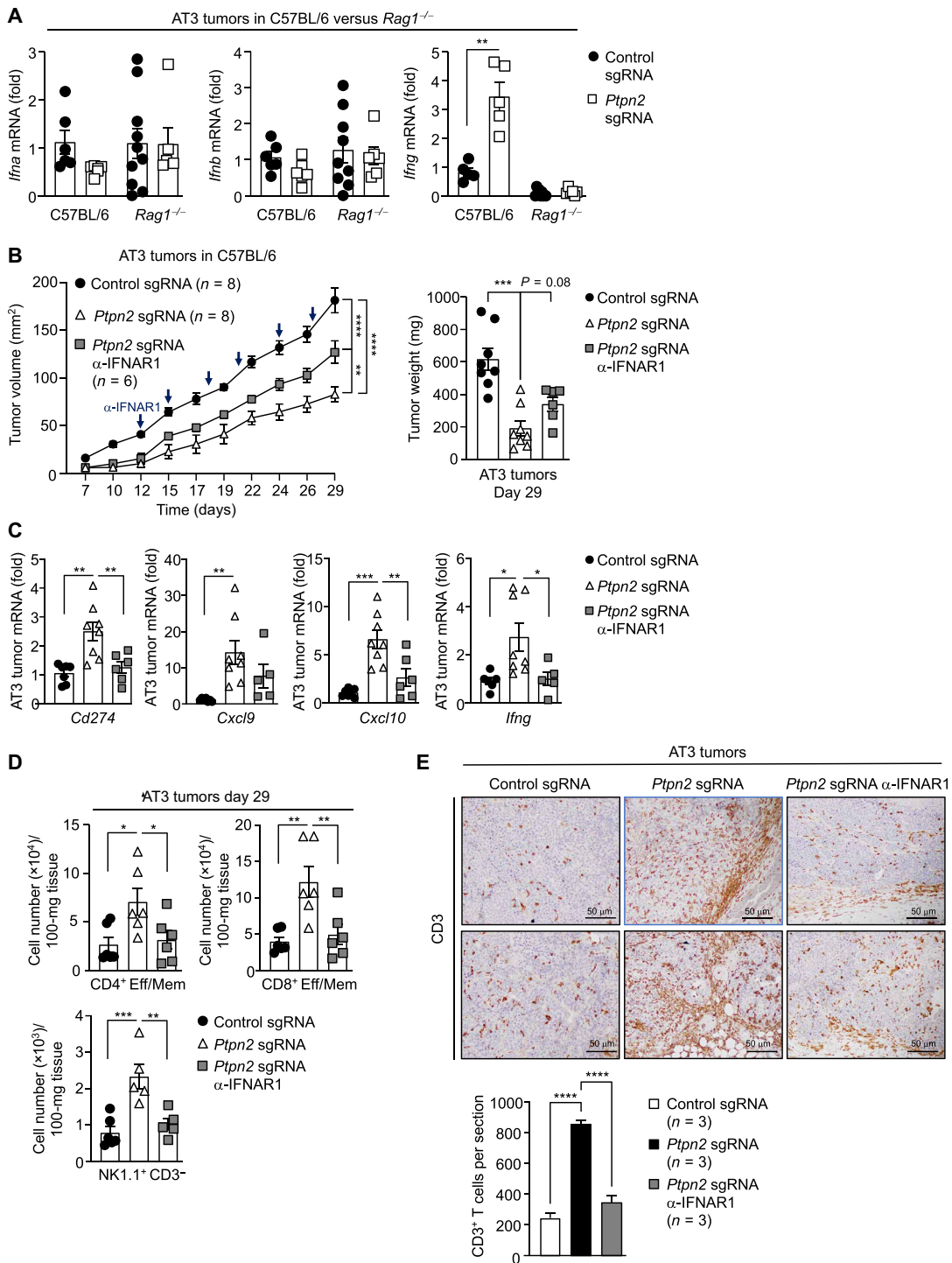


Fig. 7. The effects of PTPN2 deficiency on AT3 mammary tumor growth are reliant on IFNAR1 signaling. (A to E) AT3 control cells (control sgRNA) or those in which PTPN2 had been deleted by CRISPR RNP (*Ptpn2* sgRNA) were injected into the fourth inguinal mammary fat pads of female C57BL/6 or *Rag1*^{-/-} mice. (A) IFN α (*Ifna*), IFN β (*Ifnb*), or IFN γ (*Ifng*) mRNAs in AT3 control or PTPN2-deficient mammary tumors were assessed by qPCR. (B to E) C57BL/6 mice bearing PTPN2-deficient AT3 tumors were injected with IFNAR1 blocking antibody or PBS control every 3 days, and (B) tumor growth was monitored. (C) Tumor *Cxcl9*, *Cxcl10*, *Cd274*, and *Ifng* mRNAs were assessed by qPCR. (D) TILs including CD4 hi CD62L lo Eff/Mem phenotype and NK1.1 $^{+}$ CD3 $^{-}$ NK cells were analyzed by flow cytometry. (E) Tumors were processed for immunohistochemistry staining for CD3 (counterstained with hematoxylin). Representative results (means \pm SEM) from at least two independent experiments are shown. In (A) and (C) to (E), tumors were analyzed at end point. Tumor sizes in (A) were C57BL/6 control sgRNA, 562 \pm 97; C57BL/6 *Ptpn2* sgRNA, 205 \pm 40.2; *Rag1*^{-/-} control sgRNA, 640.9 \pm 155; and *Rag1*^{-/-} *Ptpn2* sgRNA, 555 \pm 90.1. In (A), significance was determined using two-tailed Mann-Whitney *U* test. In (B), significance was determined using two-way ANOVA test and, in (C) to (E), using one-way ANOVA test. In (E), results are representative of five mice per group, and images were taken at $\times 20$ magnification; sections from three mice per group were scored with three fields of view per section, and significance was determined using two-tailed Student's *t* test; *P \leq 0.05; **P \leq 0.01; ***P \leq 0.001; ****P \leq 0.0001.

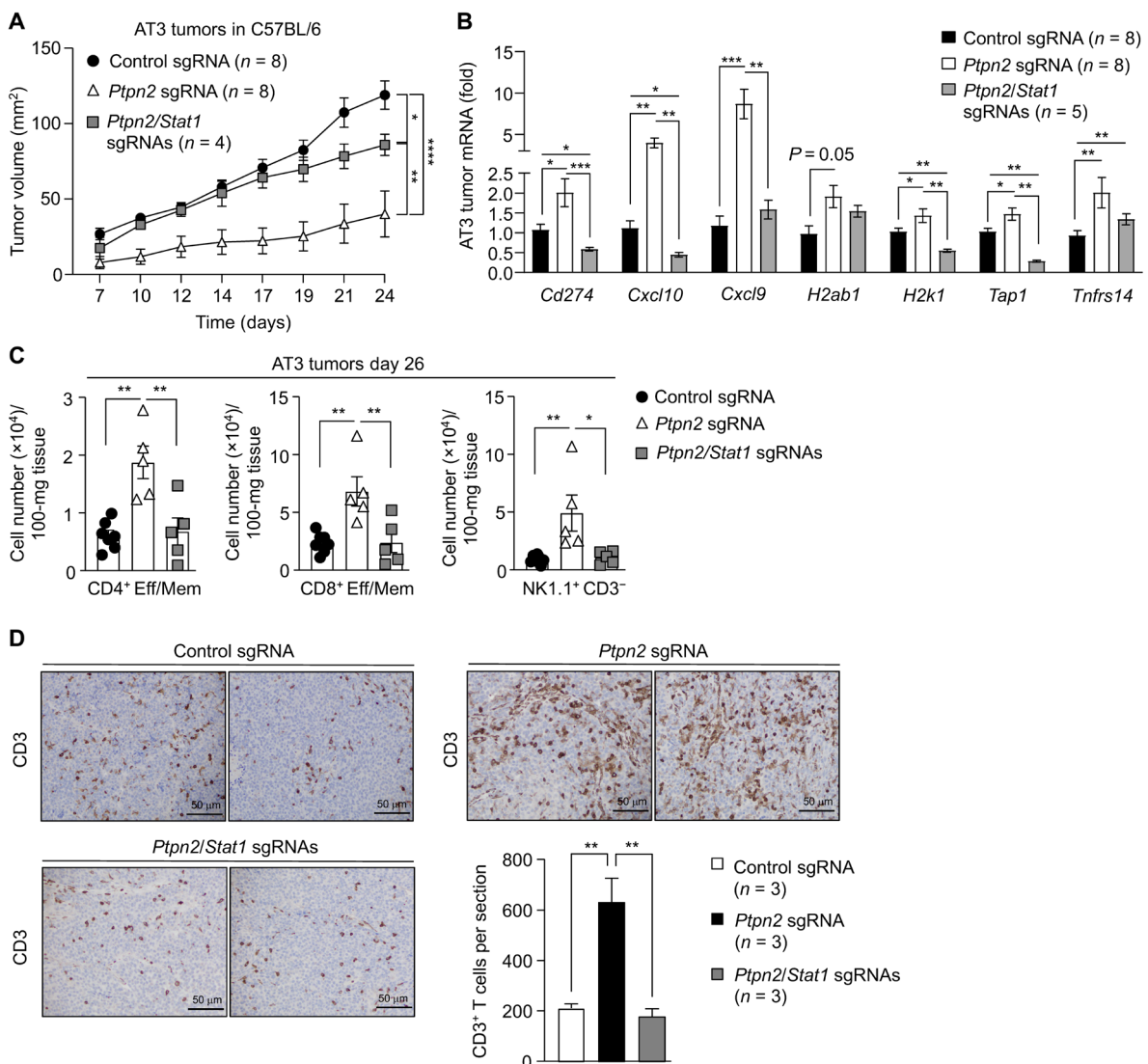


Fig. 8. The effects of PTPN2 deficiency on AT3 mammary tumor growth are reliant on the promotion of STAT-1 signaling. (A to D) AT3 control cells (control sgRNA) or those in which PTPN2 (*Ptpn2* sgRNA) or PTPN2 and STAT-1 (*Ptpn2/Stat1* sgRNA) had been deleted by CRISPR RNP were injected into the fourth inguinal mammary fat pads of female C57BL/6 mice, and (A) tumor growth was monitored. (B) Tumor STAT-1 target gene expression was assessed by qPCR. (C) TILs including CD4⁺ and CD8⁺ T cells with a CD44^{hi}CD62L^{lo} Eff/Mem phenotype and NK1.1⁺CD3⁻ NK cells were analyzed by flow cytometry. (D) Tumors were processed for immunohistochemistry staining for CD3 (counterstained with hematoxylin). Representative results (means ± SEM) from two independent experiments are shown. In (B) to (D), tumors were analyzed at end point. In (A), significance was determined using two-way ANOVA test and, in (B) to (D), using one-way ANOVA test. In (D), results are representative of five mice per group, and images were taken at ×20 magnification; sections from three mice per group were scored with three fields of view per section, and significance was determined using two-tailed Student's *t* test; **P* ≤ 0.05; ***P* ≤ 0.01; ****P* ≤ 0.001; *****P* ≤ 0.0001.

did not alter growth rates in immunodeficient *Rag1*^{−/−} mice (fig. S19C), where tumor growth otherwise exceeded that in C57BL/6 mice (fig. S19, B and C). In addition, in keeping with the elevated IFN/STAT-1 signaling and the increased *Cxcl10* expression, CD3ε⁺ T cell infiltrates were already elevated in E0771 versus AT3 tumors as assessed by immunohistochemistry (Fig. 9A); although the deletion of PTPN2 promoted the further recruitment of CD4⁺ and CD8⁺ T cells (fig. S19D), the increase was less pronounced than that in PTPN2-null AT3 tumors (Fig. 5E). In addition, NK cells in PTPN2-null versus control E0771 tumors were not significantly increased, but T_{reg}s were increased (fig. S19D). Moreover, monocytic and granulocytic MDSCs that are immunosuppressive were markedly elevated in E0771

mammary tumors when compared to AT3 tumors and increased further by the deletion of PTPN2 (fig. S20A). Consistent with the overt immunosuppressive immune landscape, tumor-infiltrating CD8⁺ T cells in PTPN2-null E0771 tumors had an exacerbated PD-1⁺Tim3⁺ exhausted phenotype (50) that was not seen in PTPN2-null AT3 tumors (fig. S20B). Together, our findings using two different syngeneic models of TNBC indicate that the deletion of PTPN2 does not enhance mammary tumor development. However, the extent to which PTPN2 deletion promotes STAT-1 signaling and thereby antitumor immunity may be dictated by independent factors that drive IFN expression and influence the inflammatory and immunosuppressive state of the tumor.

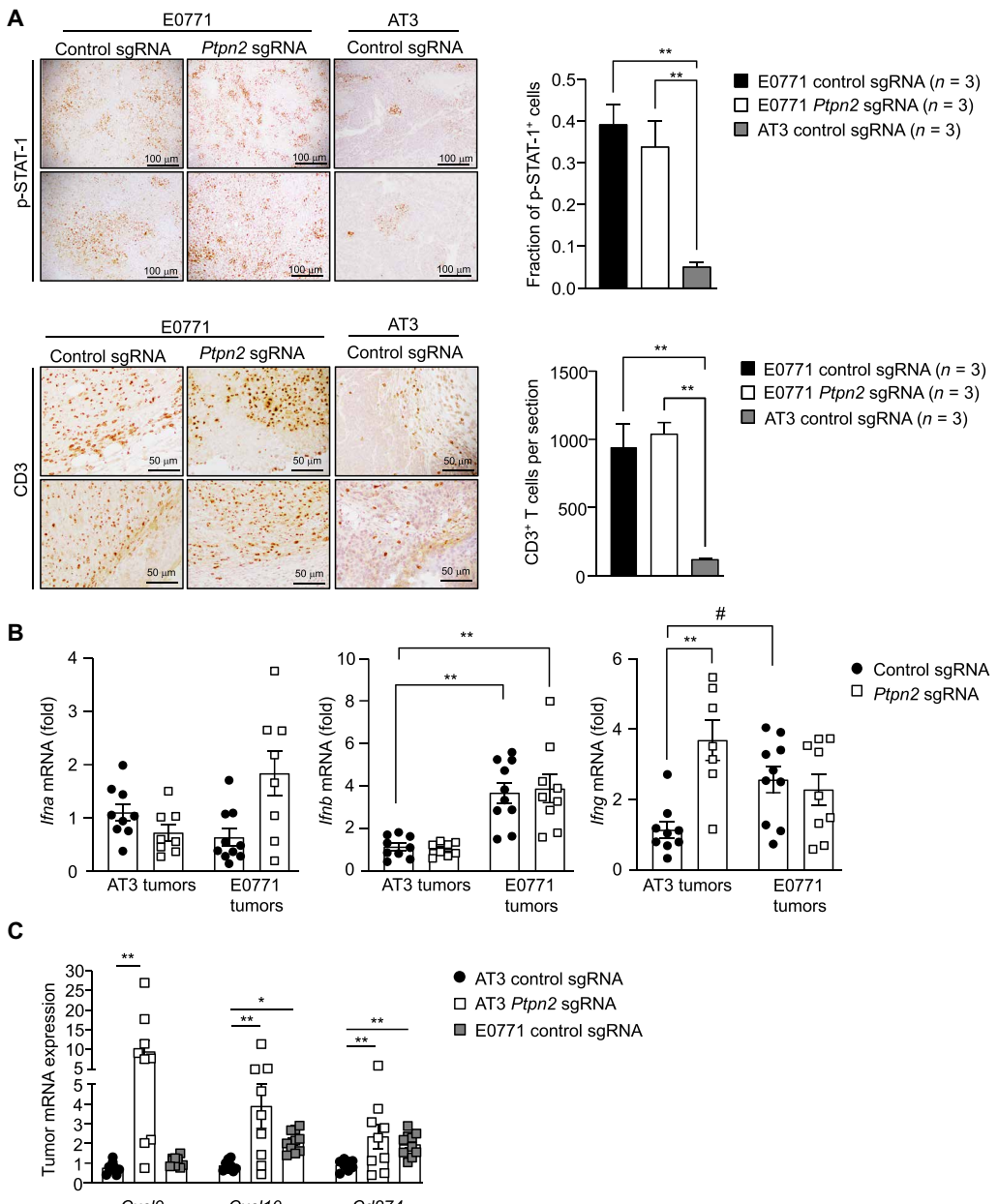


Fig. 9. E0771 mammary tumors exhibit heightened IFN expression, STAT1 signaling, and T cell infiltrates independent of PTPN2. Control tumor cells (control sgRNA) or those in which PTPN2 (*Ptpn2* sgRNA) had been deleted by CRISPR RNP were injected into the fourth inguinal mammary fat pads of female C57BL/6 mice. The resulting control or PTPN2-deficient AT3 or E0771 mammary tumors were processed for (A) immunohistochemistry staining for p-STAT1 or CD3 (counterstained with hematoxylin) or (B and C) qPCR monitoring for the expression of (B) IFN genes or (C) STAT1 target genes. Tumor sizes in (B) were AT3 control sgRNA, 594 ± 31.2 ; AT3 *Ptpn2* sgRNA, 234.4 ± 37.2 ; E0771 control sgRNA, 1020 ± 163.0 ; and E0771 *Ptpn2* sgRNA, 1006 ± 412.8 . Tumor sizes in (C) were AT3 control sgRNA, 656.0 ± 92.4 ; AT3 *Ptpn2* sgRNA, 218.8 ± 32.4 ; and E0771 control sgRNA, 746.1 ± 96.7 . Representative results (means \pm SEM) from at least two independent experiments are shown. In (B) to (C), significance was determined using one-way ANOVA test or two-tailed Mann-Whitney *U* test (#). In (A), results are representative of five mice per group, and images were taken at $\times 10$ (p-STAT1) or $\times 20$ (CD3) magnification; sections from three mice per group were scored with three fields of view per section, and significance was determined using two-tailed Student's *t* test; * or # $P \leq 0.05$; ** $P \leq 0.01$.

PTPN2 deletion in tumor cell and T cells elicits superior antitumor immunity

Previous studies have shown that, in T cells, PTPN2 has an integral role in T cell-mediated immune surveillance and that its deletion promotes T cell-mediated antitumor immunity (22, 24, 38). In particular, we have shown that deletion of PTPN2 in T cells prevents

the formation of hematological malignancies and solid tumors that otherwise occur in aged mice heterozygous for the tumor suppressor *p53* (24), which is frequently mutated in TNBC (1). Moreover, we have shown that the growth of immunogenic AT3-OVA mammary tumors implanted into the mammary fat pads of mice is markedly attenuated when PTPN2 is deleted in T cells (24). PTPN2 deletion

not only enhances TCR signaling and IL-2-induced STAT5 signaling in T cells to promote T cell activation and cytotoxicity (24) but also STAT-1 signaling to overcome T cell exhaustion (22). Accordingly, we sought to determine whether the combined targeting of PTPN2 in mammary tumor cells and T cells might not only facilitate the recruitment of T cells but also alleviate inhibitory constraints on recruited T cells to repress the growth of tumors. To this end, we implanted control or PTPN2-deficient AT3 or E0771 tumor cells into the inguinal mammary fat pads of *Ptpn2^{fl/fl}* control mice or *Lck-Cre;Ptpn2^{fl/fl}* T cell-specific PTPN2-deficient mice and assessed tumor growth (Fig. 10). Notably, we found that, whereas the deletion of PTPN2 in T cells alone was sufficient to repress the growth of AT3 mammary tumors (Fig. 10A), the combined deletion of PTPN2 in AT3 tumor cells and T cells further enhanced the repression of tumor growth (Fig. 10A). This was accompanied by the increased recruitment and/or expansion of effector T cells with enhanced cytotoxic activity (as assessed by expression of IFN γ , TNF, and granzyme B) as well as increased NK cell recruitment (Fig. 10, B and C). The increased T cell and NK cell numbers in tumors were accompanied by the promotion of STAT-1 signaling, as reflected by the increased expression of *Stat1* target genes, including *Cxcl9*, *Cxcl10*, and *Cd274* (Fig. 10D). On the other hand, although the deletion of PTPN2 in E0771 tumor cells on its own had no effect on tumor growth, PTPN2 deletion in T cells completely ablated tumor growth irrespective of PTPN2 status in tumors (Fig. 10E). Therefore, approaches aimed at targeting PTPN2 in tumors and T cells may afford a means for not only enhancing TILs and the activation and cytotoxicity of recruited T cells, but also markedly enhance the antitumor activity of T cells in TNBCs that may already be predominated by TILs.

DISCUSSION

The host immune response plays a key role in cancer progression and the response to therapy. In TNBC, the presence of TILs, especially CD8 $^+$ T cells, is widely recognized as a predictor of good prognosis in both adjuvant and neoadjuvant settings (4–6). Moreover, TNBCs with TILs and high PD-L1 show improved responses to PD-1 checkpoint blockade (51). Our findings indicate that an important factor influencing the infiltration of T cells and the expression of PD-L1 in TNBC may be PTPN2 and its negative regulation of STAT-1 signaling. Moreover, in keeping with its impact on TILs, our studies indicate that PTPN2 status may also influence survival.

We and others have reported previously that the deletion or inactivation of PTPN2 can contribute to tumorigenesis through the promotion of PTK signaling (32–35). For example, PTPN2 deletion in T-ALL drives oncogenic JAK/STAT and NUP214-ABL1 PTK signaling and tumorigenesis (35), whereas the deletion or oxidative inactivation of PTPN2 in hepatocytes in obesity promotes STAT-3 signaling and the development of hepatocellular carcinomas (32). In contrast, we found that the deletion of PTPN2 in MECs or syngeneic mammary tumors did not promote tumor formation, despite enhancing STAT-3 signaling. Although we cannot exclude the possibility that the deletion of PTPN2 in the context of other oncogenic events, such as *BRCA1* mutations or overexpressed PTKs such as epidermal growth factor receptor that are frequent in TNBC (52), might promote tumorigenesis, it is noteworthy that, even in aged multiparous mice, where oncogenic events are more likely to occur, the deletion of PTPN2 in MECs did not promote tumor formation.

The aberrant ductal and lobular structures that were otherwise readily evident in younger mice could not be detected in aged MEC-specific PTPN2-deficient mice. Instead, the deletion of PTPN2 promoted STAT-1 signaling and facilitated the recruitment of T cells to eliminate hyperplastic or dysplastic nodules and prevent tumorigenesis or repress the growth of established syngeneic mammary tumors. STAT-1 signaling is driven predominantly by type I (IFN α/β) and type II (IFN γ) IFNs; type I IFNs signal via JAK-1 and Tyk-2, which phosphorylate STAT-1 to STAT-3, whereas IFN γ signals via JAK-1 and JAK-2, which phosphorylate STAT-1 and STAT-3, to facilitate the formation of STAT-1 homodimers or heterodimers that translocate the nucleus to mediate the transcription of distinct subsets of genes (12). JAK-1 and JAK-3 and STAT-1, STAT-3, and STAT-5 can serve as direct bona fide substrates of PTPN2 (27–31). Notably, the nuclear 45-kDa variant of PTPN2 is unique in its capacity to directly dephosphorylate p-STAT-1 in the nucleus (28). Although we have not directly addressed the influence of PTPN2 deficiency on STAT-1 signaling in human breast cancer, we have shown that PTPN2 deficiency in TNBC is associated with the presence of PD-L1, a transcriptional target of STAT-1 (20). PTPN2 deficiency in TNBC was also associated with the infiltration of T cells, whereas low PTPN2 message was linked with improved survival. Using the validated monoclonal PTPN2 antibody RE5a described in this study, we have shown that both nuclear and cytoplasmic PTPN2 can otherwise be detected in TNBCs, as well as in MECs in human mammary glands, by immunohistochemistry; this was also noted previously using another validated monoclonal PTPN2 antibody, CF4 (34). Moreover, using either RE5a or CF4, both the 48- and 45-kDa PTPN2 variants can be variably detected in TNBC cell lines or tumor homogenates by immunoblotting (34). By contrast, an independent study using a commercially available polyclonal PTPN2 antibody reported that PTPN2 was predominantly cytoplasmic and rarely nuclear in breast cancer (36, 37). This study also noted that despite PTPN2 being absent in 53.3% (354 of 664) of breast cancers, especially ER $^-$ tumors, there was no correlation with TNBC (37). This discrepancy may be attributed to the inability of this antibody to detect the nuclear variant of PTPN2 by immunohistochemistry. Although our current studies do not preclude PTPN2 loss occurring and affecting the progression of other breast cancer subtypes, they reaffirm that PTPN2 deficiency does occur in TNBC and may be of functional relevance. Furthermore, although our findings need to be validated in larger cohorts of patients with breast cancer, they nonetheless suggest that, at least for a subset of TNBCs, PTPN2 status might serve not only as a marker for PD-L1 in tumor cells, but also as a marker for TILs, and that the abundance of PTPN2 may dictate the survival of patients with TNBC. Moreover, tumor cell PTPN2 status along with the mutational burden and other biomarkers might ultimately help predict immunotherapeutic efficacy in breast cancer, beyond PD-L1 expression, which is expressed at different levels, not only in tumor cells but also immune cells (1).

Beyond the potential predictive value in TNBC, our studies indicate that the inhibition of PTPN2 in at least a subset of PTPN2-positive TNBCs might ultimately help facilitate T cell recruitment and anti-tumor immunity, as well as enhance the response to PD-1 therapy. We found that the deletion of PTPN2 and the resultant STAT-1-mediated expression of T cell/NK cell chemoattractants and antigen presentation genes were associated with marked TILs and CD8 $^+$ T cell recruitment and the repression of AT3 mammary tumor growth. This occurred despite the concomitant recruitment of

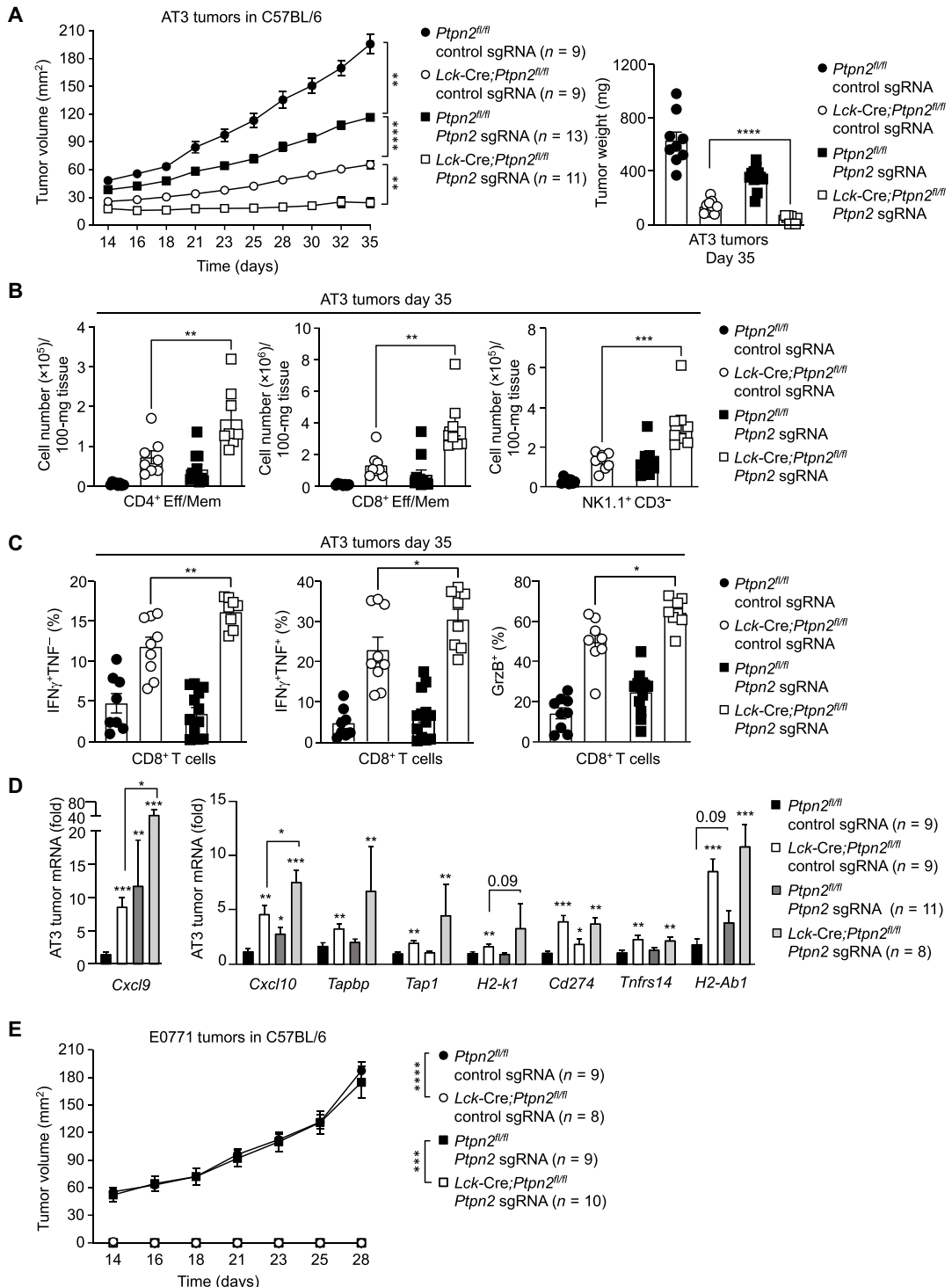


Fig. 10. PTPN2 deletion in tumor cells and T cells promotes superior antitumor immunity. (A to D) AT3 control cells (control sgRNA) or those in which PTPN2 had been deleted by CRISPR RNP (*Ptpn2* sgRNA) were injected into the fourth inguinal mammary fat pads of female *Ptpn2*^{fl/fl} versus *Lck-Cre;Ptpn2*^{fl/fl} mice, and (A) tumor growth was monitored. (B) TILs including CD4⁺ and CD8⁺ T cells with a CD44^{hi}CD62L^{lo} Eff/Mem phenotype were analyzed by flow cytometry. (C) CD8⁺ TILs were stimulated with phorbol 12-myristate 13-acetate/ionomycin in the presence of Golgi Stop/Plug and stained for intracellular IFN γ and TNF. Intracellular granzyme B (GrzB) was detected in unstimulated CD8⁺ T cell tumor infiltrates. (D) Tumor STAT-1 target genes were assessed by qPCR. (E) E0771 control sgRNA or *Ptpn2* sgRNA cells were injected into the fourth inguinal mammary fat pads of female *Ptpn2*^{fl/fl} versus *Lck-Cre;Ptpn2*^{fl/fl} mice, and tumor growth was monitored. Representative results (means \pm SEM) from at least two independent experiments are shown. In (A) and (E), significance for tumor growth was determined using two-way ANOVA test; in all other instances, significance was determined using two-tailed Mann-Whitney U test; *P \leq 0.05; **P \leq 0.01; ***P \leq 0.001; ****P \leq 0.0001.

immunosuppressive T_{regs} and MDSCs. Moreover, the promotion of STAT-1 signaling also increased the expression of immune evasion ligands, such as PD-L1, and significantly enhanced the response to α-PD-1 therapy in AT3 tumors, which were otherwise resistant to PD-1 blockade. This is consistent with the findings of others who have reported that the deletion of PTPN2 in syngeneic MC38 colon tumors or B16F10 melanomas injected into the flanks of C57BL/6 mice can enhance IFNγ-induced STAT-1 signaling and the response to immunotherapy (23). In contrast to the latter, we found that enhanced STAT-1 signaling, T cell recruitment, and PD-L1 expression were reliant on the promotion of IFNAR1 (IFNα/β) signaling. However, the extent to which PTPN2 deficiency may promote IFNα/β versus IFNγ responses is likely to be context dependent, and heightened responses to IFNγ derived from recruited T cells would be expected to further exacerbate p-STAT-1 to promote antitumor immunity. Unlike the Manguso *et al.* (23) study, the deletion of PTPN2 did not universally promote STAT-1 signaling in murine mammary tumors to affect the immune landscape. We found that the effects of PTPN2 deletion on STAT-1 signaling, TILs, and PD-L1 expression in E0771 mammary tumors were modest. Consistent with this, we found that deletion of PTPN2 did not affect the growth of E0771 tumors. These tumors already exhibited heightened STAT-1 signaling and were predominated by TILs and high PD-L1 expression. This may have been attributed to the increased IFNβ and IFNγ expression in E0771 versus AT3 tumors, which could independently drive STAT-1 signaling and T cell recruitment to negate the impact of PTPN2 deficiency. We found that IFNγ expression in E0771 tumors approximated that in PTPN2-deficient AT3 tumor cells. In pilot studies, we also found that PTPN2 deletion had no significant effect on the growth of syngeneic 4T1 mammary carcinomas, where IFNα/β expression was considerably higher than in AT3 tumors, or even E0771 tumors. Studies in rodents and humans have shown that heightened IFN signaling in TNBC is associated increased antitumor immunity, decreased metastasis, and increased survival (53, 54). Thus, the extent to which PTPN2 status may influence TILs and the response to immunotherapy in breast cancer may be dictated by the expression of components of type I/II IFN signaling pathways and/or the expression of IFN-regulated factors that drive the production of IFNs (53). Consistent with this, our studies indicate that a subset of PTPN2⁺ human TNBCs (1 of 19) can have high TILs and express PD-L1. Hence, the therapeutic targeting of PTPN2 in tumor cells alone would not be expected to universally enhance the response to immunotherapy in TNBC. Moreover, we cannot formally exclude the possibility that, in some cases, targeting PTPN2 in tumor cells alone might facilitate tumorigenesis.

On the other hand, our studies suggest that the systemic inhibition of PTPN2, or at least its inhibition in both tumor cells and T cells, might have significant benefit and facilitate both the recruitment of TILs and/or the activation of CD8⁺ T cells within the tumor to repress tumor growth. The combined deletion of PTPN2 in tumor cells and T cells enhanced the repression of AT3 mammary tumor growth and completely prevented the growth of E0771 mammary tumors that were otherwise unaffected by the deletion of PTPN2. This is consistent with previous studies that have shown that the deletion of PTPN2 in T cells can promote the activation and cytotoxicity of CD8⁺ T cells while also overcoming the exhaustion of T cells to enhance tumor immunosurveillance and prevent or repress tumor growth (22, 24). While the activation of T cells is dependent on the promotion of TCR-mediated lymphocyte-specific

protein tyrosine kinase (LCK) signaling and IL-2-induced STAT-5 signaling (24), the ability of T cells to overcome exhaustion is reliant on the promotion of IFN signaling and the expansion of a progenitor pool of exhausted T cells (22). However, other studies have also reported that the deletion of PTPN2 in antigen-presenting dendritic cells can facilitate T cell activation and repress the growth of carcinogen-induced colorectal tumors (38). Moreover, although deleting PTPN2 throughout the hematopoietic compartment in adult mice can lead to inflammatory disease and multiorgan autoimmunity (55), the deletion of PTPN2 in 50% of immune cells within the hematopoietic compartment is sufficient to repress the growth of syngeneic MC38 tumors without promoting systemic inflammation (22). Therefore, these studies point toward a potential therapeutic window for the systemic inhibition of PTPN2 to combat TNBC and possibly other cancers. In the context of TNBC at least, our studies suggest that these pharmacological approaches might not only drive IFN-STAT-1 signaling in tumor cells and thereby antigen presentation and T cell recruitment, but also help T cells overcome the immunosuppressive tumor microenvironment. These approaches may be effective on their own or in combination with other therapies, including PD-1 checkpoint blockade and potentially chemotherapy, because IFN signaling in tumor cells has been shown to contribute to the efficacy of chemotherapy in murine models of breast cancer (12, 56). Consistent with this, recently developed PTPN2 inhibitors are now in clinical trials (NCT04417465 and NCT04777994) in patients with locally advanced or metastatic tumors and are being tested alone and in combination with α-PD-1.

In summary, the results of this study point toward PTPN2 eliciting both cell autonomous and non-cell autonomous effects on TNBC development. We demonstrate that PTPN2 deficiency in tumor cells may be favorable by driving STAT-1 signaling and thereby T cell recruitment, PD-L1 expression, and antitumor immunity to enhance survival and the response to immunotherapy. Moreover, we report that the combinatorial targeting of PTPN2 in tumor cells and T cells can yield added benefit by alleviating inhibitory constraints on recruited T cells or reinvigorating otherwise exhausted preexisting intratumoral T cells to combat TNBC.

METHODS

Mice

Ptpn2^{f/f} (C57BL/6) mice have been described previously (30, 57) and were backcrossed onto the FVB/n background strain for more than 10 generations. *Lck-Cre;Ptpn2*^{f/f} [C57BL/6; *Lck-Cre*: Research Resource Identifier (RRID):International Mouse Strain Resource (IMSR)_JAX:006889] (57), *Stat1*^{f/f} (C57BL/6; IMSR catalog no. EM:09906, RRID:IMSR_EM:09906) (58), and *Ptpn2*^{-/-} [C57BL/6; RRID:Mouse Genome Informatics (MGI):5436254] (59) mice have been described previously. MMTV-CreA (FVB/n; IMSR catalog no. JAX:003551, RRID:IMSR_JAX:003551) mice (45) were provided by J. Visvader (Walter and Eliza Hall Institute, Australia) and were bred with *Ptpn2*^{f/f} (FVB/n) mice to generate MMTV-Cre; *Ptpn2*^{f/f} (FVB/n) mice. Tg(LGB-cre)74Acl/J (BLG-Cre; C57BL/6; IMSR catalog no. JAX:017836, RRID:IMSR_JAX:017836) mice were from The Jackson Laboratory (Ben Harbor, ME) and were bred with *Ptpn2*^{f/f} (C57BL/6) mice to generate BLG-Cre; *Ptpn2*^{f/f} (C57BL/6) mice. C57BL/6J (RRID:IMSR_JAX:000664) and *Rag1*^{-/-} (RRID:IMSR_APB:4878) mice were purchased from the Walter and Eliza Hall

Institute Animal Facility (Kew, Australia), whereas FVB/n and CD1 mice were from the Monash Animal Research Platform (Clayton Australia). Mice were maintained on a 12-hour light-dark cycle in temperature-controlled high-barrier facilities with free access to food and water. Experimental mice were fed a standard chow (4% fat; Barastoc, Ridley AgriProducts, Australia).

Animal ethics

All experiments were performed in accordance with the National Health and Medical Research Council (NHMRC) Australian Code of Practice for the Care and Use of Animals. All protocols were approved by the Monash University School of Biomedical Sciences Animal Ethics Committee (ethics number: MARP/2015/137) or the Peter MacCallum Animal Ethics and Experimentation Committee (ethics numbers: E572 and E604).

Materials

Rabbit p-STAT-1 (Tyr⁷⁰¹) (clone 58D6) [Research Resource Identifier (RRID): AB_2198287], rabbit p-STAT-3 (Tyr⁷⁰⁵) (clone D3A7) (RRID: AB_2255568], mouse STAT-3 (clone 124H6) (RRID: AB_331757), rabbit STAT-1 (#9172) (RRID: AB_2198300), rabbit Ki67 (clone D3B5) (RRID: AB-2687446), mouse Ki67 (clone #8D5) (RRID: AB_2797703), and rabbit Vinculin (clone E1E9V) (RRID: AB_2728768) antibodies were from Cell Signaling Technology (Danvers, MA); mouse actin (clone ACTN05) (RRID: AB_1954910) antibody was from Thermo Fisher Scientific (Waltham, MA); rabbit CK8 (clone EP1628Y) (RRID: AB_869901), mouse CK14 (clone LL002) (RRID: AB_306091), and rabbit CD3ε (clone SP7) antibodies were from Abcam (Cambridge, UK) (RRID: AB_446487); rabbit FLEX CD3ε Ready-to-Use was from Agilent Dako (RRID: AB_2732001) (Glostrup, Denmark); and mouse PTPN2 6F3 antibody was from MediMabs (Quebec, Canada). InVivoMAb anti-mouse PD-1 (clone RMP1-14), InVivoMAb anti-mouse IFNAR1 (clone MAR1-5A3), and InVivoMAb rat immunoglobulin G2a (IgG2a) isotype control were purchased from Bio X Cell (Lebanon, NH).

MEC isolation and culture

MECs were isolated as described previously (46). Briefly, the thoracic and inguinal mammary fat pads (with inguinal lymph node removed) of adult female mice were isolated, chopped with scalpels, and digested overnight at 37°C with gentle rocking with collagenase/hyaluronidase (STEMCELL Technologies, Melbourne, Australia) in Dulbecco's modified Eagle's medium (DMEM)/F12 supplemented with 5% (v/v) fetal bovine serum (FBS). Cell suspensions were then digested further in trypsin/EDTA (0.25%) for 2 min and then deoxyribonuclease I (DNase I) (5 µg/ml)/Dispase (5 U/ml) for 10 min at 37°C. Red blood cells were lysed using the Red Cell Lysis Buffer (Sigma-Aldrich, St. Louis, MO); cells were stained with Brilliant Violet 421 (BV421)-conjugated rat anti-mouse CD24 (BD Biosciences, San Jose, CA), CD29 phycoerythrin-cyanine 7 (PE-Cy7)-conjugated rat anti-mouse CD29 (BioLegend, San Diego, CA), and allophycocyanin (APC)-conjugated rat anti-mouse CD45 (BD Biosciences, San Jose, CA); and CD45⁻CD24⁺CD29^{lo} luminal and CD45⁻CD24⁺CD29^{hi} basal MECs were sorted using the BD FACSAria Fusion Cell Sorter (BD Biosciences, San Jose, CA). Where indicated, basal or luminal MECs were cultured in MEC medium [DMEM/F12 supplemented with 1% (v/v) FBS, penicillin (100 U/ml)/streptomycin (100 µg/ml), cholera toxin (100 ng/ml), hydrocortisone (500 µg/ml), insulin (10 µg/ml), and EGF (5 ng/ml)] at 37°C, 5% CO₂.

Where indicated, CD45⁻CD24⁺CD29^{lo} luminal or CD45⁻CD24⁺CD29^{hi} basal MECs from *Ptpn2*^{fl/fl} or *Ptpn2*^{fl/fl}; *Stat1*^{fl/+} (C57BL/6) mice were plated onto six-well plates precoated with the ECL Cell Attachment Matrix (Merck) in MEC medium overnight and then transduced with adenoviruses expressing Cre recombinase alone (Ad-Cre) or βGal (Ad-LacZ) (Vector Biolabs, Malvern PA) at a multiplicity of infection of 50 for 6 hours. Cells were then allowed to grow to confluence for 5 to 7 days before collection for quantitative real-time polymerase chain reaction (PCR) analysis (luminal MECs) or mammary fat pad transplantation (basal MECs).

Mammary fat pad transplantation

Mammary fat pad transplants were performed as described previously (46, 60). Briefly, 3-week-old female C57BL/6 or FVB/n mice were anesthetized with 2% (v/v) isoflurane in oxygen (1.5 liter/min), and a small inverted Y incision was made at the lower trunk. The three main blood vessels running to the mammary gland around the proximal lymph node were cauterized to prevent excessive bleeding, and the bridge connecting mammary fat pads 4 and 5 was severed using the cauterizer. The region of the mammary fat pad between the nipple and before the proximal lymph node was removed (cleared), and CD45⁻CD24⁺CD29^{hi} basal MECs were injected (5000 cells/10 µl) into the remaining portion of the epithelium-free mammary fat pad between the inguinal lymph node and the midline. From each donor (pooled samples from three donors), three recipients were transplanted, with each recipient receiving wild-type basal MECs into one fat pad and *Ptpn2*-null basal MECs into the contralateral mammary fat pad. MEC outgrowths were assessed after 12 weeks.

Mammary fat pad whole-mount carmine alum staining, immunohistochemistry, and immunofluorescence microscopy

Mammary gland development was assessed by whole-mount carmine alum staining. Briefly, inguinal fat pads were dissected, stretched on a microscope slide, fixed overnight in 4% neutral buffered formalin, and incubated in a series of phosphate-buffered saline (PBS), 70% ethanol, and three 100% ethanol washes, 1 hour each. Whole mounts were then stained in carmine alum [0.2% (w/v) carmine and 0.5% (w/v) aluminum potassium sulfate] overnight, rinsed in distilled water, and dehydrated in 70 and then 100% ethanol, followed by xylene before being imaged in methyl salicylate. Whole mounts were scanned using an Olympus BX51 microscope and analyzed using OlyVIA software (Olympus, Tokyo, Japan) measuring ductal diameters.

For immunohistochemistry and immunofluorescence microscopy, inguinal fat pads were formalin-fixed and paraffin-embedded in formalin. Sections were dewaxed in Histosol (Trajan Scientific Australia) for 3 × 5 min and dehydrated in ethanol (3 × 5 min), and antigens were retrieved in tris/EDTA (pH 8.0) buffer for 10 min in a pressure cooker (70 kPa). For immunohistochemistry, endogenous peroxidase activity was blocked in 3% H₂O₂ for 10 min, and sections were blocked in 2% (w/v) bovine serum albumin (BSA) in 50 mM tris-HCl (pH 7.2) for 1 hour at room temperature and primary antibodies p-STAT-1 (Tyr⁷⁰¹) (1:500; Cell Signaling Technology), p-STAT-3 (Tyr⁷⁰⁵) (1:150; Cell Signaling Technology), Ki67 (1:500; clone D3B5, Cell Signaling Technology), and STAT-1 (1:200; Cell Signaling Technology), and α-PTPN2 monoclonal 6F3 diluted in 50 mM tris-HCl (pH 7.2) and 1% (w/v) BSA was incubated overnight (4°C) and visualized using anti-rabbit or anti-mouse secondary antibodies conjugated with horseradish peroxidase (HRP)-labeled

polymer (Dako EnVision+ System- HRP Labeled Polymer, Dako Products, Agilent, Santa Clara, CA) plus 3,3'-diaminobenzidine (DAB) chromogenic staining. Cells were counterstained with hematoxylin for 1 min before rinsing in distilled water. Slides were then dehydrated in ethanol (3×5 min), cleared in Histosol (3×5 min), and mounted in DPX Mountant (Sigma-Aldrich, St. Louis, MO). Sections were scanned using the Aperio Scanscope AT Turbo (Aperio, Vista, CA).

For immunofluorescence microscopy, sections were blocked in 5% normal goat serum in 0.4% Triton X-100 in PBS for 1 hour and incubated with primary antibodies p-STAT-1 (Tyr⁷⁰¹) (1:500; Cell Signaling Technology), α -CK8 (1:500; Abcam), α -CK14 (1:500; Abcam), α -CD3 ϵ (1:250; Dako) and α -PTPN2 monoclonal 6F3 diluted in 0.1% Triton X-100 in PBS overnight at 4°C and then goat anti-rabbit IgG (H + L) Alexa Fluor 488 or goat anti-mouse IgG (H + L) Alexa Fluor 568 (1:1000; Invitrogen, Thermo Fisher Scientific, Waltham, MA) secondary antibodies for 1 hour at room temperature. Nuclei were counterstained with 4',6-diamidino-2-phenylindole (DAPI) before mounting in Dako mounting medium (Dako Products, Agilent, Santa Clara, CA). Fluorescence sections were scanned and imaged using the Nikon C1 Inverted Microscope based on Nikon Eclipse Ti (Nikon Instruments, Melville, NY).

Mammary tumor immunohistochemistry and immunofluorescence microscopy

For immunohistochemical analysis of mammary tumors, tumors were dissected and fixed in buffered formalin solution for 48 hours. Tissues were embedded in paraffin, and 4- μ m sections of the entire block were prepared. After deparaffinization and rehydration, sections were subjected to antigen retrieval in tris/EDTA buffer (pH 8.0) at 120°C for 5 min. Sections were blocked with 1.5% (v/v) horse (Ki67) or goat (p-STAT-1, p-STAT-3, and CD3) serum in PBS for 30 min at room temperature and incubated overnight (4°C) with p-STAT-1 (Tyr⁷⁰¹) (1:500; Cell Signaling Technology), p-STAT-3 (Tyr⁷⁰⁵) (1:200; Cell Signaling Technology), Ki67- (1:400; clone #8D5, Cell Signaling Technology), or CD3-positive cells (1:200; Abcam). After washing with PBS, p-STAT-1, p-STAT-3, Ki67-, or CD3-positive cells were visualized using rabbit (p-STAT-1, p-STAT-3, and CD3) or mouse (Ki67) IgG VECTORSTAIN ABC Elite and DAB Peroxidase Substrate Kits (Vector Laboratories, UK). Sections were counterstained with hematoxylin and imaged on an Olympus CX43 microscope (Olympus, Tokyo, Japan).

Tumor cell culture

The C57BL/6 mouse breast carcinoma cell line E0771 (a gift from R. Anderson, Peter MacCallum Cancer Centre) and the C57BL/6 mouse mammary tumor cell line AT3 have been previously described (47, 48). *Ptpn2* was deleted in E0771 cells, and *Ptpn2* and *Stat1* were deleted in AT3 cells using CRISPR RNP-based gene editing. Cells were transfected with recombinant Cas9 (74 pmol; Alt-R S.p. Cas9 Nuclease V3, Integrated DNA Technologies) precomplexed with synthetic single guide RNAs (sgRNAs) (600 pmol; Synthego) targeting the *Ptpn2* locus (*Ptpn2*; 5'-AAGAAGUUACAUUAA-CAC-3') or the *Stat1* locus (*Stat1* sgRNA#1, 5'-GGUCGCAAACGAG-ACAUCAU-3'; *Stat1* sgRNA#2, 5'-GAGGAGGUCAUGGAAGCGGA-3') or nontargeting sgRNAs (5'-GCACUACCAGAGCUAACUCA-3') as a control using the P3 Primary Cell 4D-Nucleofector X Kit (Lonza, Basel Switzerland) according to the manufacturer's instructions; *Stat1* sgRNA#1 was used in in vivo studies. AT3 and

E0771 tumor cells were cultured in high-glucose DMEM supplemented with 10% (v/v) FBS, L-glutamine (2 mM), penicillin (100 U/ml)/streptomycin (100 μ g/ml), MEM nonessential amino acids (0.1 mM), sodium pyruvate (1 mM), Hepes (10 mM), and 2-mercaptoethanol (50 μ M) at 37°C, 10% CO₂. Human TNBC CAL-120 (a gift from R. J. Daly, Monash University, Australia), MFM223 (a gift from R. J. Daly, Monash University, Australia), MDA-MB-468, MDA-MB-453, MDA-MB-231, and MDA-MB-157 cell lines (American Type Culture Collection) were cultured in RPMI 1640 supplemented with 10% (v/v) FBS, penicillin (100 U/ml)/streptomycin (100 μ g/ml), and bovine insulin (10 μ g/ml) at 37°C, 10% CO₂. Where indicated, tumor cells were serum-starved in 0.1% (v/v) FBS for 4 hours and stimulated with IL-6 (10 ng/ml) or IFN γ (2 ng/ml) at 37°C, 10% CO₂ for the indicated times and processed for immunoblotting or quantitative real-time PCR. For immunoblotting, cells were washed with ice-cold PBS and lysed in ice-cold radioimmunoprecipitation assay (RIPA) lysis buffer [50 mM Hepes (pH 7.4), 1% (v/v) Triton X-100, 1% (v/v) sodium deoxycholate, 0.1% (v/v) SDS, 150 mM NaCl, 10% (v/v) glycerol, 1.5 mM MgCl₂, 1 mM EGTA, 50 mM sodium fluoride, pepstatin A (1 μ g/ml), aprotinin (5 μ g/ml), 1 mM benzamidine, 1 mM phenylmethylsulfonyl fluoride, and 1 mM sodium vanadate], clarified by centrifugation (16,000g, 10 min, 4°C), resolved by SDS-polyacrylamide gel electrophoresis (10%), transferred to polyvinylidene difluoride (Merck, Darmstadt, Germany), and immunoblotted.

Syngeneic tumor models

Eight- to 10-week-old female C57BL/6 mice, *Ptpn2*^{f/f} versus *Lck*-Cre; *Ptpn2*^{f/f} mice, or *Rag1*^{-/-} mice were anesthetized with isoflurane and injected orthotopically with 5×10^5 tumor cells resuspended in 20 μ l of PBS into the fourth mammary fat pad. Palpable tumors were measured using calipers until they reached 200 mm² and then extracted for quantitative PCR, histology, or flow cytometry. For IFNAR1-blocking experiments, mice inoculated with AT3 *Ptpn2* sgRNA cells were treated with mouse IFNAR1 antibody (200 μ g per mouse in 200 μ l of PBS via intraperitoneal injection) starting day 12 post-tumor cell injection and continued until control tumors reached 200 mm². Tumors were then extracted for quantitative PCR, histology, or flow cytometry.

Immune checkpoint blockade

C57BL/6 mice bearing large (~50 mm²) AT3 tumors received four intraperitoneal injections of α -PD-1 (200 μ g in 200 μ l of PBS; clone RMP1-14) or rat IgG2a isotype control (100 μ g in 200 μ l of PBS, Bio X Cell) every 4 days. Mice were euthanized at the experimental end point (200 mm² of tumor size) and survival was monitored.

Analysis of TILs

Tumors were digested at 37°C for 30 min using a cocktail of collagenase type IV (1 mg/ml) (Worthington Biochemicals) and DNaseI (0.02 mg/ml) (Sigma-Aldrich) in DMEM supplemented with 2% (v/v) FBS. Cells were passed through a 70- μ m cell strainer (BD Biosciences) and processed for flow cytometry. Cells were stained with the specified antibodies on ice for 30 min and analyzed using a Fortessa or Symphony (BD Biosciences). Data were analyzed using FlowJo 10.7.1 (Tree Star Inc.) software. For cell quantification, a known number of Flow-Count Fluorospheres (Beckman Coulter) was added to samples before analysis. Dead cells were excluded with propidium iodide (1 μ g/ml; Sigma-Aldrich) or LIVE/DEAD Fixable Near IR stain

(Thermo Fisher Scientific). For the detection of intracellular FoxP3, the Foxp3/Transcription Factor Staining Buffer Set (eBioscience) was used according to the manufacturer's instructions. For the detection of intracellular TNF and IFN γ , TILs were incubated with phorbol 12-myristate 13-acetate (50 ng/ml; Sigma-Aldrich) and ionomycin (1 μ g/ml; Sigma-Aldrich) in the presence of BD GolgiStop and BD GolgiPlug for 4 hours in complete T cell medium [RPMI 1640 supplemented with 10% (v/v) FBS, L-glutamine (2 mM), penicillin (100 U/ml)/streptomycin (100 μ g/ml), MEM nonessential amino acids (0.1 mM), sodium pyruvate (1 mM), Hepes (10 mM), and 2- β -mercaptoethanol (50 μ M)]. For the detection of intracellular granzyme B, TILs were left unstimulated. Cells were fixed, stained for CD4 and CD8 and then permeabilized with the BD Cytofix/Cytoperm Kit according to the manufacturer's instructions, intracellularly stained for TNF and IFN γ or granzyme B, and processed for flow cytometry.

The following antibodies from BD Biosciences, BioLegend, or eBioscience were used for flow cytometry: BV421-conjugated TCR- β (H57-597; BioLegend catalog no. 109229, RRID:AB_10933263), PE-Cy7-conjugated or APC-conjugated CD4 (RM4-5; BD Biosciences catalog no. 561099, RRID:AB_2034007; BD Biosciences catalog no. 553051, RRID:AB_398528), BV711 or APC-conjugated CD8 (53-6.7; BioLegend catalog no. 100759, RRID:AB_2563510; BD Biosciences catalog no. 553035, RRID:AB_398527), PE-conjugated CD25 (P61; BD Biosciences catalog no. 553866, RRID:AB_395101), BV786-conjugated CD44 (IM7; BD Biosciences catalog no. 563736, RRID:AB_2738395), fluorescein isothiocyanate (FITC) or APC-Cy7-conjugated CD45 (30-F11; Thermo Fisher Scientific catalog no. 11-0451-85, RRID:AB_465051; BD Biosciences catalog no. 557659, RRID:AB_396774), BV421-conjugated CD62L (Mel-14; BioLegend catalog no. 104435, RRID:AB_10900082), BV711-conjugated CD11b (M1/70; BioLegend catalog no. 101241, RRID:AB_11218791), PE-conjugated F4/80 (BM8; BD Biosciences catalog no. 565410, RRID:AB_2687527), PE-Cy7-conjugated NK1.1 (PK136; BD Biosciences catalog no. 552878, RRID:AB_394507), BV605-conjugated Ly6G/C (RB6-8C5; BioLegend catalog no. 108439, RRID:AB_2562333), FITC-conjugated Ly6G (1A8; BD Biosciences catalog no. 551460, RRID:AB_394207), APC-conjugated TNF (MP6-XT22; BD Biosciences catalog no. 561062, RRID:AB_2034022), PE-Cy7-conjugated IFN γ (XMG1.2; BD Biosciences catalog no. 557649, RRID:AB_396766), BV421-granzyme B (GB11; BD Biosciences catalog no. 563389, RRID:AB_2738175), BV421-conjugated FoxP3 (MF23; BD Biosciences catalog no. 562996, RRID:AB_2737940), or FITC-conjugated FoxP3 (FKJ-16s; Thermo Fisher Scientific catalog no. 11-5773-80, RRID:AB_465242).

Quantitative real-time PCR

RNA was extracted using RNAzol reagent (Sigma-Aldrich, St. Louis, MO), and RNA quality and quantity were assessed using NanoDrop 2000 (Thermo Fisher Scientific, Waltham MA). mRNA was reverse-transcribed using the High-Capacity cDNA Reverse Transcription Kit (Applied Biosystems, Thermo Fisher Scientific, Waltham, MA) and processed for quantitative real-time PCR using the Fast SYBR Green Master Mix (Applied Biosystems, Thermo Fisher Scientific, Waltham MA). PrimePCR SYBR Green Assay (Bio-Rad, Hercules, CA) primer sets were used to perform quantitative real-time PCRs for *Cxcl9* (qMmuCID0023784), *Cxcl10* (qMmuCED0049500), *Tapbp* (qMmuCEP0035035), *Tap1* (qMmuCEP0057739), *Tnfrsf14* (qMmuCIP0031437), H2ab1 (qMmuCIP0029038), *Bcl2*

(qMmuCEP0042187), *Ccl5* (qMmuCEP0057452), *Ccnd1* (qMmuCIP0035710), *Slc2a1* (qMmuCEP0037046), *Hif1a* (qMmuCIP0030996), *Iil10* (qMmuCEP0053393), *Iil6* (qMmuCEP0054186), *Vegfa* (qMmuCEP0042478), *Myc* (qMmuCIP0028153), *Tgfb1* (qMmuCEP0053152), *Cd274* (qMmuCED0044192), *H2k1* (qMmuCEP0034842), *Ifna1* (qMmuCEP0062630), *Ifnb1* (qMmuCEP0058870), and *Ifng* (qMmuCID0006268). Relative gene expression was determined by normalization to the house-keeping gene *Rps18* (qMmuCED0045430), and $\Delta\Delta C_t$ analysis was performed.

PTPN2 antibody generation

Recombinant human 45-kDa PTPN2 used for immunization was produced in *Escherichia coli* BL21(DE3) cells transformed with pET-TC45 plasmid and purified by Diethylaminoethyl (DEAE) cellulose and carboxymethyl (CM)-Sepharose chromatography as described previously (61). Mouse monoclonal PTPN2 antibodies were generated by the Monash Antibody Technologies Facility (Monash University, Australia). Briefly 6-week-old CD1 mice were injected intraperitoneally with recombinant human 45-kDa PTPN2 (12.8 μ g per mouse) in Sigma Adjuvant System (Sigma-Aldrich, St. Louis, MO), with three boosts given every 2 weeks for 6 weeks. After the final boost, primary splenocytes were isolated, fused with myeloma Sp2/0 cells, and plated onto 96-well plates to generate antibody-producing hybridomas. Supernatants from the resulting hybridomas were screened for PTPN2 antigen-positive lines using microarrays (printed using the Arraviet Super Marathon, Array-Jet, Roslin, UK), standard enzyme-linked immunosorbent assays, and by immunohistochemistry monitoring for PTPN2 staining in control versus PTPN2-deficient HeLa cells as described previously (34). Specific PTPN2 clones were subcloned to monoclonality by limiting dilution. The clonal hybridoma line RE5a was expanded and adapted to serum-free and suspension culture, and the human PTPN2-specific RE5a antibody was purified by affinity chromatography using the Millipore Protein G Sepharose Fast Flow (Merck, Darmstadt, Germany). The RE5a isotope was IgG3 κ , as determined using the IsoStrip Mouse Monoclonal Antibody Isotyping Kit (Roche, Basel, Switzerland) according to the manufacturer's instructions.

PTPN2 antibody validation

The binding region for the RE5a antibody on human 45-kDa PTPN2 was assessed by Western blot analysis monitoring for immunoreactivity toward recombinant human 45-kDa PTPN2 used for immunization or recombinant glutathione S-transferase-PTPN2 fusion proteins encompassing either full-length human PTPN2 (residues 1 to 387), a series of C-terminal truncation mutants (1 to 376, 1 to 359, and 1 to 349), or the C-terminal noncatalytic domain (318 to 381) of PTPN2 produced in *E. coli* BL21(DE3) cells and purified using glutathione Sepharose 4 Fast Flow (Merck, Darmstadt, Germany) as described previously (61, 62). The specificity of the RE5a antibody for PTPN2 was assessed by immunoblotting and immunohistochemistry using control HeLa cells and PTPN2-deficient HeLa cells described previously (34). Briefly, PTPN2-deficient cells HeLa cells were transduced with control or PTPN2 (TRCN0000002783)-specific MISSION shRNA lentiviral particles (Sigma-Aldrich) and selected in puromycin as described previously (34). To generate tumor xenografts for immunohistochemical analyses, control and PTPN2-deficient HeLa cells were injected into the flanks of BALB/c *nu/nu* mice, and the resultant tumors (1000 mm³) were extracted,

fixed in buffered formalin, and paraffin-embedded, and sections were cut and immediately processed for RE5a immunohistochemistry (as described for tumor immunohistochemistry studies) and counterstained with hematoxylin. The specificity of the RE5a antibody for PTPN2 in human TNBCs was assessed by immunoblotting-clarified (16,000g) RIPA lysates of the immortalized human TNBC cell lines CAL-120, MDA-MB-468, MDA-MB-453, MDA-MB-231, MFM223, and MDA-MB-157.

TNBC immunohistochemistry

Ethics approval for the use of TNBC tissues was obtained from the Monash University Human Research Ethics Committee (25836). Twenty-eight female cases of ER-negative, PR-negative, and HER2-negative (triple negative) invasive carcinoma not otherwise specified (World Health Organization, 2018) of breast (average age of 73 years old) were obtained through the archives of the Alfred Health Anatomical Pathology Department.

Immunoperoxidase staining performed on the tissue blocks included RE5a (Monash Antibody Technologies Facility, Monash University), PD-L1 (PD-L1 IHC 22C3 pharmDX, Agilent, Santa Clara, CA), and FLEX polyclonal rabbit anti-human CD3 Ready-to-Use using the DAKO EnVision FLEX, High pH (Dako Omnis) GV800 on the Dako Autostainer (Dako Products, Agilent, Santa Clara, CA). Serial sections were taken from each block for additional immunoperoxidase staining. All sections had control positive and negative tissue on the same slide. Cases were analyzed as positive with RE5a when there was nuclear and/or cytoplasmic immunoreactivity; internal controls of PTPN2-positive lymphocytes were used. Cases were analyzed as positive for PD-L1 when any membrane staining of tumor cells was seen; internal controls of positive macrophages were used. Stromal TIL analysis was performed using the consensus scoring recommendations (63). For analysis, when the TIL score was >50%, the case was deemed as high TILs; CD3 immunoreactivity was used verify the extent of CD3⁺ T cell infiltrates.

Microarray data analyses

Previously generated microarray gene expression data from the tumors of 243 patients with stage I to III breast cancer (cohort 1) (39) or from 462 patients with stage I to III breast cancer (<https://tcga-data.nci.nih.gov/tcga/>) (cohort 2) were interrogated to correlate PTPN2 expression to patient outcome and clinical variables. Among cohort 1, 189 (78%) patients were ER-positive, 168 (69%) were PR-positive, and 41 (17%) were HER2-positive. One hundred twenty-one (50%) were lymph node-positive, the mean tumor size was 23 mm, and the mean patient age was 44. Among cohort 2, 358 (77%) patients were ER-positive, 299 (65%) were PR-positive, and 99 (21%) were HER2-positive; 229 (50%) were lymph node-positive, and the mean patient age was 58.9. We also interrogated a previously generated microarray gene expression data from the tumors of 238 patients with stage I to III TNBC (40) and correlated PTPN2 expression to patient outcome; 108 (46%) were lymph node-positive, the mean tumor size was 24.3 mm, and the mean patient age was 54.6.

Gene expression data analysis was performed in R software with additional Bioconductor packages (www.r-project.org and www.bioconductor.org). The primary end point for the survival analyses was breast cancer-specific survival, which was measured from the date of diagnosis to death from breast cancer or otherwise censored at the time of the last follow-up visit or at non-disease-related death.

Times to disease-specific deaths were plotted as Kaplan-Meier survival curves. Cox proportional hazards regression was used for univariate analysis of the prognostic impact of PTPN2 expression. For statistical analysis, SPSS (version 15.0.1; SPSS Inc., Chicago, IL) software was used.

Statistical analyses

Unless otherwise indicated, statistical analyses were performed with GraphPad Prism software 8.4.3 using the nonparametric two-tailed Mann-Whitney *U* test, the parametric two-tailed Student's *t* test, or the one-way or two-way analysis of variance (ANOVA) using Tukey or Sidak post hoc comparison. *P* < 0.05 was considered as significant (**P* ≤ 0.05, ***P* ≤ 0.01, and ****P* ≤ 0.001).

SUPPLEMENTARY MATERIALS

Supplementary material for this article is available at <https://science.org/doi/10.1126/sciadv.abk3338>

[View/quest a protocol for this paper from Bio-protocol.](#)

REFERENCES AND NOTES

1. A. C. Garrido-Castro, N. U. Lin, K. Polyak, Insights into molecular classifications of triple-negative breast cancer: Improving patient selection for treatment. *Cancer Discov.* **9**, 176–198 (2019).
2. C. Denkert, S. Loibl, A. Noske, M. Roller, B. M. Muller, M. Komor, J. Budczies, S. Darb-Esfahani, R. Kronenwett, C. Hanusch, C. von Torne, W. Weichert, K. Engels, C. Solbach, I. Schrader, M. Dietel, G. von Minckwitz, Tumor-associated lymphocytes as an independent predictor of response to neoadjuvant chemotherapy in breast cancer. *J. Clin. Oncol.* **28**, 105–113 (2010).
3. S. Adams, R. J. Gray, S. Demaria, L. Goldstein, E. A. Perez, L. N. Shulman, S. Martino, M. Wang, V. E. Jones, T. J. Saphner, A. C. Wolff, W. C. Wood, N. E. Davidson, G. W. Sledge, J. A. Sparano, S. S. Badve, Prognostic value of tumor-infiltrating lymphocytes in triple-negative breast cancers from two phase III randomized adjuvant breast cancer trials: ECOG 2197 and ECOG 1199. *J. Clin. Oncol.* **32**, 2959–2966 (2014).
4. M. V. Dieci, M. C. Mathieu, V. Guarneri, P. Conte, S. Delaloge, F. Andre, A. Goubar, Prognostic and predictive value of tumor-infiltrating lymphocytes in two phase III randomized adjuvant breast cancer trials. *Ann. Oncol.* **26**, 1698–1704 (2015).
5. S. Loi, D. Drubay, S. Adams, G. Pruneri, P. A. Francis, M. Lacroix-Triki, H. Joensuu, M. V. Dieci, S. Badve, S. Demaria, R. Gray, E. Munzone, J. Lemonnier, C. Sotiriou, M. J. Piccart, P. L. Kellokumpu-Lehtinen, A. Vingiani, K. Gray, F. Andre, C. Denkert, R. Salgado, S. Michiels, Tumor-infiltrating lymphocytes and prognosis: A pooled individual patient analysis of early-stage triple-negative breast cancers. *J. Clin. Oncol.* **37**, 559–569 (2019).
6. P. Savas, R. Salgado, C. Denkert, C. Sotiriou, P. K. Darcy, M. J. Smyth, S. Loi, Clinical relevance of host immunity in breast cancer: From TILs to the clinic. *Nat. Rev. Clin. Oncol.* **13**, 228–241 (2016).
7. M. Miyashita, H. Sasano, K. Tamaki, H. Hirakawa, Y. Takahashi, S. Nakagawa, G. Watanabe, H. Tada, A. Suzuki, N. Ohuchi, T. Ishida, Prognostic significance of tumor-infiltrating CD8⁺ and FOXP3⁺ lymphocytes in residual tumors and alterations in these parameters after neoadjuvant chemotherapy in triple-negative breast cancer: A retrospective multicenter study. *Breast Cancer Res.* **17**, 124 (2015).
8. P. Sharma, J. P. Allison, Immune checkpoint targeting in cancer therapy: Toward combination strategies with curative potential. *Cell* **161**, 205–214 (2015).
9. S. L. Topalian, C. G. Drake, D. M. Pardoll, Immune checkpoint blockade: A common denominator approach to cancer therapy. *Cancer Cell* **27**, 450–461 (2015).
10. P. Schmid, S. Adams, H. S. Rugo, A. Schneeweiss, C. H. Barrios, H. Iwata, V. Dieras, R. Hegg, S. A. Im, G. Shaw Wright, V. Henschel, L. Molinero, S. Y. Chui, R. Funke, A. Husain, E. P. Winer, S. Loi, L. A. Emens, I. M. T. Investigators, Atezolizumab and Nab-paclitaxel in advanced triple-negative breast cancer. *N. Engl. J. Med.* **379**, 2108–2121 (2018).
11. S. Loi, S. Dushyantha, P. A. Beavis, R. Salgado, C. Denkert, P. Savas, S. Combs, D. L. Rimm, J. M. Giltnane, M. V. Estrada, V. Sanchez, M. E. Sanders, R. S. Cook, M. A. Pilkinton, S. A. Mallal, K. Wang, V. A. Miller, P. J. Stephens, R. Yelenksy, F. D. Doimi, H. Gomez, S. V. Ryzhov, P. K. Darcy, C. L. Arteaga, J. M. Balko, RAS/MAPK activation is associated with reduced tumor-infiltrating lymphocytes in triple-negative breast cancer: Therapeutic cooperation between MEK and PD-1/PD-L1 immune checkpoint inhibitors. *Clin. Cancer Res.* **22**, 1499–1509 (2016).
12. B. S. Parker, J. Rautela, P. J. Hertzog, Antitumour actions of interferons: Implications for cancer therapy. *Nat. Rev. Cancer* **16**, 131–144 (2016).

13. A. Widschwendter, S. Tonko-Geymayer, T. Welte, G. Daxenbichler, C. Marth, W. Doppler, Prognostic significance of signal transducer and activator of transcription 1 activation in breast cancer. *Clin. Cancer Res.* **8**, 3065–3074 (2002).
14. M. E. Legrier, I. Bieche, J. Gaston, A. Beurdeley, V. Yvonne, O. Deas, A. Thuleau, S. Chateau-Joubert, J. L. Servely, S. Vacher, M. Lassalle, S. Depil, G. C. Tucker, J. J. Fontaine, M. F. Poupon, S. Roman-Roman, J. G. Judde, D. Decaudin, S. Cairo, E. Marangoni, Activation of IFN/STAT1 signalling predicts response to chemotherapy in oestrogen receptor-negative breast cancer. *Br. J. Cancer* **114**, 177–187 (2016).
15. C. Yau, L. Esserman, D. H. Moore, F. Waldman, J. Sninsky, C. C. Benz, A multigene predictor of metastatic outcome in early stage hormone receptor-negative and triple-negative breast cancer. *Breast Cancer Res.* **12**, R85 (2010).
16. P. J. Klover, W. J. Muller, G. W. Robinson, R. M. Pfeiffer, D. Yamaji, L. Hennighausen, Loss of STAT1 from mouse mammary epithelium results in an increased Neu-induced tumor burden. *Neoplasia* **12**, 899–905 (2010).
17. S. R. Chan, W. Vermi, J. Luo, L. Lucini, C. Rickert, A. M. Fowler, S. Lonardi, C. Arthur, L. J. Young, D. E. Levy, M. J. Welch, R. D. Cardiff, R. D. Schreiber, STAT1-deficient mice spontaneously develop estrogen receptor α -positive luminal mammary carcinomas. *Breast Cancer Res.* **14**, R16 (2012).
18. A. E. Koromilas, V. Sexl, The tumor suppressor function of STAT1 in breast cancer. *Jakstat* **2**, e23353 (2013).
19. N. Nagarsheth, M. S. Wicha, W. Zou, Chemokines in the cancer microenvironment and their relevance in cancer immunotherapy. *Nat. Rev. Immunol.* **17**, 559–572 (2017).
20. A. Garcia-Diaz, D. S. Shin, B. H. Moreno, J. Saco, H. Escuin-Ordinas, G. A. Rodriguez, J. M. Zaretsky, L. Sun, W. Hugo, X. Wang, G. Parisi, C. P. Saus, D. Y. Torrejon, T. G. Graeber, B. Comin-Anduix, S. Hu-Lieskovian, R. Damoiseaux, R. S. Lo, A. Ribas, Interferon receptor signaling pathways regulating PD-L1 and PD-L2 expression. *Cell Rep.* **19**, 1189–1201 (2017).
21. J. L. Bencic, B. H. Xu, Y. Qiu, T. J. Wu, H. Dada, C. Twyman-Saint Victor, L. Cucolo, D. S. M. Lee, K. E. Pauken, A. C. Huang, T. C. Gangadhar, R. K. Amaravadi, L. M. Schuchter, M. D. Feldman, H. Ishwaran, R. H. Vonderheide, A. Maity, E. J. Wherry, A. J. Minn, Tumor interferon signaling regulates a multigenic resistance program to immune checkpoint blockade. *Cell* **167**, 1540–1554.e12 (2016).
22. M. W. LaFleur, T. H. Nguyen, M. A. Coxe, B. C. Miller, K. B. Yates, J. E. Gillis, D. R. Sen, E. F. Gudiano, R. Al Abosy, G. J. Freeman, W. N. Haining, A. H. Sharpe, PTPN2 regulates the generation of exhausted CD8(+) T cell subpopulations and restrains tumor immunity. *Nat. Immunol.* **20**, 1335–1347 (2019).
23. R. T. Manguso, H. W. Pope, M. D. Zimmer, F. D. Brown, K. B. Yates, B. C. Miller, N. B. Collins, K. Bi, M. W. LaFleur, V. R. Juneja, S. A. Weiss, J. Lo, D. E. Fisher, D. Miao, E. Van Allen, D. E. Root, A. H. Sharpe, J. G. Doench, W. N. Haining, In vivo CRISPR screening identifies Ptpn2 as a cancer immunotherapy target. *Nature* **547**, 413–418 (2017).
24. F. Wiede, K. H. Lu, X. Du, S. Liang, K. Hochheiser, G. T. Dodd, P. K. Goh, C. Kearney, D. Meyran, P. A. Beavis, M. A. Henderson, S. L. Park, J. Waithman, S. Zhang, Z. Y. Zhang, J. Oliaro, T. Gebhardt, P. K. Darcy, T. Tiganis, PTPN2 phosphatase deletion in T cells promotes anti-tumour immunity and CAR T-cell efficacy in solid tumours. *EMBO J.* **39**, e103637 (2020).
25. T. Tiganis, A. M. Bennett, Protein tyrosine phosphatase function: The substrate perspective. *Biochem. J.* **402**, 1–15 (2007).
26. S. Bussières-Marmen, A. P. Hutchins, A. Schirbel, N. Rebert, T. Tiganis, C. Fiocchi, D. Miranda-Saavedra, M. L. Tremblay, Characterization of PTPN2 and its use as a biomarker. *Methods* **65**, 239–246 (2014).
27. P. D. Simoncini, A. Lee-Loy, D. L. Barber, M. L. Tremblay, C. J. McGlade, The T cell protein tyrosine phosphatase is a negative regulator of janus family kinases 1 and 3. *Curr. Biol.* **12**, 446–453 (2002).
28. J. ten Hoeve, M. J. Ibarra-Sánchez, Y. Fu, W. Zhu, M. Tremblay, M. David, K. Shuai, Identification of a nuclear Stat1 protein tyrosine phosphatase. *Mol. Cell. Biol.* **22**, 5662–5668 (2002).
29. B. J. Shields, C. Hauser, P. E. Bukczynska, N. W. Court, T. Tiganis, DNA replication stalling attenuates tyrosine kinase signaling to suppress S phase progression. *Cancer Cell* **14**, 166–179 (2008).
30. K. Loh, A. Fukushima, X. Zhang, S. Galic, D. Briggs, P. J. Enriori, S. Simonds, F. Wiede, A. Reichenbach, C. Hauser, N. A. Sims, K. K. Bence, S. Zhang, Z. Y. Zhang, B. Kahn, B. G. Neel, Z. B. Andrews, M. A. Cowley, T. Tiganis, Elevated hypothalamic TCPTP in obesity contributes to cellular leptin resistance. *Cell Metab.* **14**, 684–699 (2011).
31. E. N. Gurzov, M. Tran, M. A. Fernandez-Rojo, T. L. Merry, X. Zhang, Y. Xu, A. Fukushima, M. J. Waters, M. J. Watt, S. Andrikopoulos, B. G. Neel, T. Tiganis, Hepatic oxidative stress promotes insulin-STAT5 signaling and obesity by inactivating protein tyrosine phosphatase N2. *Cell Metab.* **20**, 85–102 (2014).
32. M. Grohmann, F. Wiede, G. T. Dodd, E. N. Gurzov, G. J. Ooi, T. Butt, A. A. Rasmussen, S. Kaur, T. Gulati, P. K. Goh, A. E. Treloar, S. Archer, W. A. Brown, M. Muller, M. J. Watt, O. Ohara, C. A. McLean, T. Tiganis, Obesity drives STAT-1-dependent NASH and STAT-3-dependent HCC. *Cell* **175**, 1289–1306.e20 (2018).
33. H. Lee, M. Kim, M. Baek, L. D. Morales, I. S. Jang, T. J. Slaga, J. DiGiovanni, D. J. Kim, Targeted disruption of TC-PTP in the proliferative compartment augments STAT3 and AKT signaling and skin tumor development. *Sci. Rep.* **7**, 45077 (2017).
34. B. J. Shields, F. Wiede, E. N. Gurzov, K. Wee, C. Hauser, H. J. Zhu, T. J. Molloy, S. A. O'Toole, R. J. Daly, R. L. Sutherland, C. A. Mitchell, C. A. McLean, T. Tiganis, TCPTP regulates SFK and STAT3 signaling and is lost in triple-negative breast cancers. *Mol. Cell. Biol.* **33**, 557–570 (2013).
35. M. Kleppe, I. Lahortiga, T. El Chaar, K. De Keersmaecker, N. Mentens, C. Graux, K. Van Roosbroeck, A. A. Ferrando, A. W. Langerak, J. P. Meijerink, F. Sigaux, T. Haferlach, I. Wlodarska, P. Vandenberghe, J. Soulier, J. Cools, Deletion of the protein tyrosine phosphatase gene PTPN2 in T-cell acute lymphoblastic leukemia. *Nat. Genet.* **42**, 530–535 (2010).
36. E. Karlsson, C. Veenstra, J. Garsjo, B. Nordenskjold, T. Fornander, O. Stal, PTPN2 deficiency along with activation of nuclear Akt predict endocrine resistance in breast cancer. *J. Cancer Res. Clin. Oncol.* **145**, 599–607 (2019).
37. C. Veenstra, E. Karlsson, S. M. Mirwani, B. Nordenskjold, T. Fornander, G. Perez-Tenorio, O. Stal, The effects of PTPN2 loss on cell signalling and clinical outcome in relation to breast cancer subtype. *J. Cancer Res. Clin. Oncol.* **145**, 1845–1856 (2019).
38. E. Katkeviciute, L. Hering, A. Montalban-Arques, P. Busenhart, M. Schwarzfischer, R. Manzini, J. Conde, K. Attrott, S. Lang, G. Rogler, E. Naschberger, V. S. Schellerer, M. Sturzl, A. Rickenbacher, M. Turina, A. Weber, S. Leibl, G. E. Leventhal, M. Levesque, O. Boyman, M. Scharl, M. R. Spalinger, Protein tyrosine phosphatase nonreceptor type 2 controls colorectal cancer development. *J. Clin. Invest.* **131**, e140281 (2021).
39. M. J. van de Vijver, Y. D. He, L. J. van't Veer, H. Dai, A. A. Hart, D. W. Voskuil, G. J. Schreiber, J. L. Peterse, C. Roberts, M. J. Marton, M. Parrish, D. Atsma, A. Witteveen, A. Glas, L. Delahaye, T. van der Velde, H. Bartelink, S. Rodenhuis, E. T. Rutgers, S. H. Friend, R. Bernards, A gene-expression signature as a predictor of survival in breast cancer. *N. Engl. J. Med.* **347**, 1999–2009 (2002).
40. P. Jezequel, O. Kerdraon, H. Hondermarck, C. Guerin-Charbonnel, H. Lasla, W. Gouraud, J. L. Canon, A. Gombos, F. Dalenc, S. Delaloge, J. Lemonnier, D. Loussouarn, V. Verrielle, M. Campone, Identification of three subtypes of triple-negative breast cancer with potential therapeutic implications. *Breast Cancer Res.* **21**, 65 (2019).
41. S. Selbert, D. J. Bentley, D. W. Melton, D. Rannie, P. Lourenco, C. J. Watson, A. R. Clarke, Efficient BLG-Cre mediated gene deletion in the mammary gland. *Transgenic Res.* **7**, 387–398 (1998).
42. G. Molyneux, F. C. Geyer, F. A. Magnay, A. McCarthy, H. Kendrick, R. Natrajan, A. Mackay, A. Grigoriadis, A. Tutt, A. Ashworth, J. S. Reis-Filho, M. J. Smalley, BRCA1 basal-like breast cancers originate from luminal epithelial progenitors and not from basal stem cells. *Cell Stem Cell* **7**, 403–417 (2010).
43. A. McCarthy, K. Savage, A. Gabriel, C. Naceur, J. S. Reis-Filho, A. Ashworth, A mouse model of basal-like breast carcinoma with metaplastic elements. *J. Pathol.* **211**, 389–398 (2007).
44. B. Lloyd-Lewis, O. B. Harris, C. J. Watson, F. M. Davis, Mammary stem cells: Premise, properties, and perspectives. *Trends Cell Biol.* **27**, 556–567 (2017).
45. K. U. Wagner, R. J. Wall, L. St-Onge, P. Gruss, A. Wynshaw-Boris, L. Garrett, M. Li, P. A. Furth, L. Hennighausen, Cre-mediated gene deletion in the mammary gland. *Nucleic Acids Res.* **25**, 4323–4330 (1997).
46. M. Shackleton, F. Vaillant, K. J. Simpson, J. Stingl, G. K. Smyth, M. L. Asselin-Labat, L. Wu, G. J. Lindeman, J. E. Visvader, Generation of a functional mammary gland from a single stem cell. *Nature* **439**, 84–88 (2006).
47. T. J. Stewart, S. I. Abrams, Altered immune function during long-term host-tumor interactions can be modulated to retard autochthonous neoplastic growth. *J. Immunol.* **179**, 2851–2859 (2007).
48. C. N. Johnstone, Y. E. Smith, Y. Cao, A. D. Burrows, R. S. Cross, X. Ling, R. P. Redvers, J. P. Doherty, B. L. Eckhardt, A. L. Natoli, C. M. Restall, E. Lucas, H. B. Pearson, S. Deb, K. L. Britt, A. Rizzitelli, J. Li, J. H. Harmey, N. Pouliot, R. L. Anderson, Functional and molecular characterisation of EO771.LMB tumours, a new C57BL/6-mouse-derived model of spontaneously metastatic mammary cancer. *Dis. Model. Mech.* **8**, 237–251 (2015).
49. L. B. John, C. Devaud, C. P. Duong, C. S. Yong, P. A. Beavis, N. M. Haynes, M. T. Chow, M. J. Smyth, M. H. Kershaw, P. K. Darcy, Anti-PD-1 antibody therapy potently enhances the eradication of established tumors by gene-modified T cells. *Clin. Cancer Res.* **19**, 5636–5646 (2013).
50. C. U. Blank, W. N. Haining, W. Held, P. G. Hogan, A. Kallies, E. Lugli, R. C. Lynn, M. Philip, A. Rao, N. P. Restifo, A. Schietinger, T. N. Schumacher, P. L. Schwartzberg, A. H. Sharpe, D. E. Speiser, E. J. Wherry, B. A. Youngblood, D. Zehn, Defining 'T cell exhaustion'. *Nat. Rev. Immunol.* **19**, 665–674 (2019).
51. R. K. Beckers, C. I. Selingar, R. Vilain, J. Madore, J. S. Wilmott, K. Harvey, A. Holliday, C. L. Cooper, E. Robbins, D. Gillett, C. W. Kennedy, L. Gluch, H. Carmalt, C. Mak, S. Warrier, H. E. Gee, C. Chan, A. McLean, E. Walker, C. M. McNeil, J. M. Beith, A. Swarbrick, R. A. Scolyer, S. A. O'Toole, Programmed death ligand 1 expression in triple-negative breast cancer is associated with tumour-infiltrating lymphocytes and improved outcome. *Histopathology* **69**, 25–34 (2016).
52. J. Crown, J. O'Shaughnessy, G. Gullo, Emerging targeted therapies in triple-negative breast cancer. *Ann. Oncol.* **23** (Suppl. 6), vi56–vi65 (2012).
53. B. N. Bidwell, C. Y. Slaney, N. P. Withana, S. Forster, Y. Cao, S. Loi, D. Andrews, T. Mikeska, N. E. Mangan, S. A. Samaraijiwa, N. A. de Weerd, J. Gould, P. Argani, A. Moller, M. J. Smyth,

- R. L. Anderson, P. J. Hertzog, B. S. Parker, Silencing of Ifr7 pathways in breast cancer cells promotes bone metastasis through immune escape. *Nat. Med.* **18**, 1224–1231 (2012).
54. N. K. Brockwell, J. Rautela, K. L. Owen, L. J. Gearing, S. Deb, K. Harvey, A. Spurling, D. Zanker, C. L. Chan, H. E. Cumming, N. T. Deng, J. M. Zakhour, H. M. Duivenvoorden, T. Robinson, M. Harris, M. White, J. Fox, C. Ooi, B. Kumar, J. Thomson, N. Potasz, A. Swarbrick, P. J. Hertzog, T. J. Molloy, S. O'Toole, V. Ganju, B. S. Parker, Tumor inherent interferon regulators as biomarkers of long-term chemotherapeutic response in TNBC. *NPJ Precis. Oncol.* **3**, 21 (2019).
55. F. Wiede, F. Sacirbegovic, Y. A. Leong, D. Yu, T. Tiganis, PTPN2-deficiency exacerbates T follicular helper cell and B cell responses and promotes the development of autoimmunity. *J. Autoimmun.* **76**, 85–100 (2017).
56. A. Sistigu, T. Yamazaki, E. Vacchelli, K. Chaba, D. P. Enot, J. Adam, I. Vitale, A. Goubar, E. E. Baracco, C. Remedios, L. Fend, D. Hannani, L. Aymeric, Y. Ma, M. Niso-Santano, O. Kepp, J. L. Schultze, T. Tutting, F. Belardelli, L. Bracci, V. La Sorsa, G. Ziccheddu, P. Sestili, F. Urbani, M. Delorenzi, M. Lacroix-Triki, V. Quidville, R. Conforti, J. P. Spano, L. Pusztai, V. Poirier-Colame, S. Delalogue, F. Penault-Llorca, S. Ladoire, L. Arnould, J. Cyrtà, M. C. Dessoliers, A. Eggermont, M. E. Bianchi, M. Pittet, C. Engblom, C. Pfirschke, X. Preville, G. Uze, R. D. Schreiber, M. T. Chow, M. J. Smyth, E. Proietti, F. Andre, G. Kroemer, L. Zitvogel, Cancer cell-autonomous contribution of type I interferon signaling to the efficacy of chemotherapy. *Nat. Med.* **20**, 1301–1309 (2014).
57. F. Wiede, B. J. Shields, S. H. Chew, K. Kyparissoudis, C. van Vliet, S. Galic, M. L. Tremblay, S. M. Russell, D. I. Godfrey, T. Tiganis, T cell protein tyrosine phosphatase attenuates T cell signaling to maintain tolerance in mice. *J. Clin. Invest.* **121**, 4758–4774 (2011).
58. B. Wallner, N. R. Leitner, R. M. Vielhascher, E. Kernbauer, T. Kolbe, M. Karaghiosoff, T. Rulicke, T. Decker, M. Muller, Generation of mice with a conditional Stat1 null allele. *Transgenic Res.* **21**, 217–224 (2012).
59. F. Wiede, S. Hui Chew, C. van Vliet, I. J. Poultton, K. Kyparissoudis, T. Sasmono, K. Loh, M. L. Tremblay, D. I. Godfrey, N. A. Sims, T. Tiganis, Strain-dependent differences in bone development, myeloid hyperplasia, morbidity and mortality in Ptpn2-deficient mice. *PLOS ONE* **7**, e36703 (2012).
60. K. L. Britt, H. Kendrick, J. L. Regan, G. Molyneux, F. A. Magnay, A. Ashworth, M. J. Smalley, Pregnancy in the mature adult mouse does not alter the proportion of mammary epithelial stem/progenitor cells. *Breast Cancer Res.* **11**, R20 (2009).
61. L. Hao, T. Tiganis, N. K. Tonks, H. Charbonneau, The non-catalytic C-terminal segment of the T cell protein tyrosine phosphatase regulates activity via an intramolecular mechanism. *J. Biol. Chem.* **272**, 29322–29329 (1997).
62. T. Tiganis, A. J. Flint, S. A. Adam, N. K. Tonks, Association of the T-cell protein tyrosine phosphatase with nuclear import factor p97. *J. Biol. Chem.* **272**, 21548–21557 (1997).
63. R. Salgado, C. Denkert, S. Demaria, N. Sirtaine, F. Klauschen, G. Pruneri, S. Wienert, G. Van den Eynden, F. L. Baehner, F. Penault-Llorca, E. A. Perez, E. A. Thompson, W. F. Symmans, A. L. Richardson, J. Brock, C. Criscitiello, H. Bailey, M. Ignatiadis, G. Floris, J. Sparano, Z. Kos, T. Nielsen, D. L. Rimm, K. H. Allison, J. S. Reis-Filho, S. Loibl, C. Sotiriou, G. Viale, S. Badve, S. Adams, K. Willard-Gallo, S. Loi; International TILs Working Group 2014, The evaluation of tumor-infiltrating lymphocytes (TILs) in breast cancer: Recommendations by an International TILs Working Group 2014. *Ann. Oncol.* **26**, 259–271 (2015).

Acknowledgments: We thank A. Ziegler for antibody screening, T. Butt for technical support, and the Monash Antibody Technologies Facility for antibody generation. **Funding:** This work was supported by the Austrian Science Fund FWF (SFB F6101 and F6106 to M.M.), Worldwide Cancer Research (18-0045 to T.T. and C.M.), the U.S. Army Department of Defense (BC200609 to T.T.), and the NHMRC of Australia (APP1003037 to T.T.). **Author contributions:** T.T. conceived and conceptualized the study, designed the experiments, wrote the manuscript, and interpreted the data with intellectual input and approval from all authors. P.K.G., F.W., and M.N.Z. conceptualized and designed experiments, conducted and analyzed most of the experiments, and contributed to the reviewing and editing of the manuscript. Other authors performed and/or analyzed experiments and/or contributed to the reviewing and editing of the manuscript. **Competing interests:** F.W. and T.T. are inventors on a pending patent related to this work filed by Monash University (no. US20210052648A1, filed 08 September 2020, published 25 February 2021). The authors declare that they have no other competing interests.

Data and materials availability: All data needed to evaluate the conclusions in the paper are present in the paper and/or the Supplementary Materials. The *Stat1^{fl/fl}* mice can be provided by the University of Veterinary Medicine, Vienna pending scientific review and a completed material transfer agreement. Requests for the *Stat1^{fl/fl}* mice should be submitted to M.M., University of Veterinary Medicine, Vienna.

Submitted 7 July 2021

Accepted 24 December 2021

Published 23 February 2022

10.1126/sciadv.abk3338